



Jennions, S., Thomas, E., Schmidt, D., Lunt, D., & Ridgwell, A. (2015). Changes in benthic ecosystems and ocean circulation in the Southeast Atlantic across Eocene Thermal Maximum 2. *Paleoceanography*. 10.1002/2015PA002821

Peer reviewed version

Link to published version (if available):
[10.1002/2015PA002821](https://doi.org/10.1002/2015PA002821)

[Link to publication record in Explore Bristol Research](#)
PDF-document

University of Bristol - Explore Bristol Research

General rights

This document is made available in accordance with publisher policies. Please cite only the published version using the reference above. Full terms of use are available:
<http://www.bristol.ac.uk/pure/about/ebr-terms.html>

Take down policy

Explore Bristol Research is a digital archive and the intention is that deposited content should not be removed. However, if you believe that this version of the work breaches copyright law please contact open-access@bristol.ac.uk and include the following information in your message:

- Your contact details
- Bibliographic details for the item, including a URL
- An outline of the nature of the complaint

On receipt of your message the Open Access Team will immediately investigate your claim, make an initial judgement of the validity of the claim and, where appropriate, withdraw the item in question from public view.

30 **Abstract**

31 Eocene Thermal Maximum 2 (ETM2) occurred ~1.8 Myr after the Paleocene Eocene Thermal
32 Maximum (PETM) and, like the PETM, was characterized by a negative carbon isotope excursion and
33 warming. We combined benthic foraminiferal and sedimentological records for Southeast Atlantic Sites
34 1263 (1500 m paleodepth) and 1262 (3600 m paleodepth) to show that benthic foraminiferal diversity
35 and accumulation rates declined more precipitously and severely at the shallower site during peak
36 ETM2. As the sites are in close proximity, differences in surface productivity cannot have caused this
37 differential effect. Instead, we infer that changes in ocean circulation across ETM2 may have produced
38 more pronounced warming at intermediate depths (Site 1263). The effects of warming include
39 increased metabolic rates, a decrease in effective food supply and increased deoxygenation, thus
40 potentially explaining the more severe benthic impacts at Site 1263. In response, bioturbation may have
41 decreased more at Site 1263 than at Site 1262, differentially affecting bulk carbonate records. We use a
42 sediment-enabled Earth system model to test whether a reduction in bioturbation and/or the likely
43 reduced carbonate saturation of more poorly ventilated waters can explain the more extreme excursion
44 in bulk $\delta^{13}\text{C}$ and sharper transition in wt% CaCO_3 at Site 1263. We find that both enhanced
45 acidification and reduced bioturbation during the ETM2 peak are needed to account for the observed
46 features. Our combined ecological and modelling analysis illustrates the potential role of ocean
47 circulation changes in amplifying local environmental changes and driving temporary, but drastic, loss
48 of benthic biodiversity and abundance.

49 **Index Terms & Keywords:**

50 **Eocene, hyperthermal event, benthic ecosystem, ocean circulation change**

51

52 **1. Introduction**

53 Potential environmental impacts of increasing atmospheric CO₂ concentrations include warming,
54 increased intensity of the hydrological cycle and nutrient influx into the oceans, ocean stratification,
55 ocean acidification, and increased hypoxia [*Caldeira & Wickett, 2003; Hutchins et al., 2007; Solomon*
56 *et al., 2009; Coma et al., 2009; Keeling et al., 2010; Durack et al., 2012; Pörtner et al., 2014*], any or
57 all of which may affect organisms and ecosystems. However, anticipating the biotic response to
58 these multiple, potentially synergistic environmental parameters is challenging [*Bopp et al., 2013;*
59 *Melzner et al 2013; Norris et al., 2013; Pörtner et al., 2014*]. The response of species and ecosystems
60 to changing environments has been, and continues to be, tested in mostly single-driver laboratory
61 experiments, producing short-term, species-specific, and mainly physiological information (e.g.,
62 *Kroeker et al., [2010], Pörtner et al., [2014]*). Such experiments are valuable, but reflect neither the
63 complexity of the natural environment nor the adaptability of organisms on long time scales. Records
64 of periods of past climate change, can, however, provide a detailed, quantifiable account of biotic
65 response (e.g. *Hönisch et al., [2012], Speijer et al., [2012]*). A series of global warming and carbon
66 release events ('hyperthermals') of variable intensity, occurring superimposed upon gradually rising
67 global temperatures during the early- to mid- Palaeogene [*Thomas and Zachos, 2000; Cramer, 2003;*
68 *Lourens et al., 2005; Sluijs et al., 2007a*] provide us with the potential for just such a test.

69 The best studied and largest of the hyperthermals is the Palaeocene Eocene Thermal Maximum
70 (PETM), with a variety of proxies indicating global warming due to emission of isotopically light
71 carbon into the ocean-atmosphere [*Dunkley Jones et al., 2013*]. In addition to warming, surface waters
72 experienced rapid and sustained surface water ocean acidification [*Penman et al., 2014*]. Oxygenation
73 may have decreased globally during the PETM in response to warming, hydrological change and
74 carbon cycle feedbacks [*Winguth et al., 2012*], with bottom water deoxygenation common
75 along continental margins [*Thomas, 1998; Nicolo et al., 2010*], and the inferred occurrence of a broad
76 expansion of oxygen minimum zones in the open ocean [*Zhou et al., 2014*]. Bottom water
77 deoxygenation may have occurred at some open ocean southeast Atlantic sites [*Chun et al., 2010; Post*
78 *et al., 2015*], but not in the Pacific [*Pälike et al., 2014*]. Nutrient availability and productivity may
79 have increased in marginal basins, but decreased in pelagic settings, although discussion is still on-
80 going due to regional difference in nutrient availability and productivity [*Gibbs et al., 2006; Thomas,*
81 *2007; Winguth et al., 2012; Schneider et al., 2013; Sluijs et al., 2014; Stassen et al., 2015*]. Knowledge

82 of these changes is important because it allows exploration of the relationships between ecological
83 sensitivity and environmental change.

84 In response to PETM environmental changes, phytoplankton and zooplankton expanded their
85 ranges towards higher latitudes [*Kelly et al.*, 1996; *Thomas and Shackleton*, 1996; *Crouch et al.*, 2001;
86 *Bralower*, 2002; *Hollis*, 2006; *Shuijs et al.*, 2006; *Schneider et al.*, 2013]. Species turnover, combined
87 with evolution of short lived ‘excursion taxa’ resulted in transient changes in assemblage composition
88 of marine pelagic groups [*Kelly et al.*, 1996; *Gibbs et al.*, 2006; *Raffi et al.*, 2006; *Luciani et al.*, 2007].
89 In addition, the PETM induced one of the largest recorded extinction events of deep-sea benthic
90 foraminifera (35-40 % species extinction) [*Thomas*, 1998, 2007; *Alegret et al.*, 2010].

91 In contrast, much less is known about the marine biotic response to the smaller hyperthermals. We
92 focus here on Eocene Thermal Maximum 2 (ETM2, previously described as H1), which occurred at
93 ~53.7 Ma, i.e., about 1.8 Myr after the PETM [*Stap et al.*, 2010a; *Westerhold et al.*, 2012; *Littler et al.*,
94 2014]. The ETM2 has been identified globally in marine and terrestrial records [*Lourens et al.*, 2005;
95 *Stein et al.*, 2006; *Nicolo et al.*, 2007; *Agnini et al.*, 2009; *Stap et al.*, 2009, 2010a, 2010b; *Shuijs et al.*,
96 2009; *Clementz et al.*, 2011; *Abels et al.*, 2012; *d’Haenens et al.*, 2012; *Dedert et al.*, 2012; *Slotnick et*
97 *al.*, 2012]. The event is also well-documented in drill sites on Walvis Ridge (SE Atlantic Ocean) along
98 a depth transect from ~3500 (Site 1262) to ~1500 m (Site 1263) paleodepth [*Zachos et al.*, 2004a,
99 2004b]. The full duration of the ETM2 is estimated at ~100 kyr [*Stap et al.*, 2009], with a CIE
100 magnitude of around -1.5 ‰, i.e., about half that of the PETM at the same site [*McCarren et al.*, 2008].
101 The accompanying carbonate dissolution was also less severe [*Stap et al.*, 2009], with a reduction by
102 ~80 % during the peak of the event (‘ETM2 horizon’, 40-55 ka after its onset) [*Lourens et al.*, 2005;
103 *Stap et al.*, 2009] rather than complete dissolution of CaCO₃ as during the PETM [*Zachos et al.*, 2005].
104 Peak warming was estimated at 3-4 °C for bottom waters [*Stap et al.*, 2010b], whereas estimates of
105 surface water warming vary between ~2 °C in the South Atlantic [*Lourens et al.*, 2005; *Stap et al.*,
106 2009, 2010a], ~2-2.5 °C in the North Atlantic [*d’Haenens et al.*, 2014] and ~4°C in Arctic [*Shuijs et al.*,
107 2009], compared to 5-6 °C averaged globally for the PETM [*Zachos et al.*, 2005; *Shuijs et al.*, 2007b;
108 *Dunkley Jones et al.*, 2013]. Unlike the PETM, there was no significant extinction of benthic
109 foraminifers associated with ETM2, despite possible evolution of susceptible species in the 1.8 Myr
110 between the events [*Lourens et al.*, 2005; *Stap et al.*, 2010a].

111 In this paper, we assess the biotic response of benthic ecosystems to ETM2 environmental changes
112 at Walvis Ridge. We analyse a series of coupled climate and conceptual Earth system modelling
113 experiments in order to explore the potential causes and consequences of benthic ecological change.

114

115 **2. Materials and Methods**

116 *2.1. Samples*

117 We obtained samples from two sites drilled during ODP Leg 208, Walvis Ridge, South Atlantic, Sites
118 1262 (palaeodepth 3,600 m) and 1263 (palaeodepth 1,500 m) [Zachos *et al.*, 2004a, 2004b] (Figure 1).
119 Cores from Hole 1262A and 1263C were sampled between 116.75-117.40 mcd and 294.27-295.53 mcd
120 respectively [Lourens *et al.*, 2005; Stap *et al.*, 2009], corresponding
121 to topmost Chron C24r, nannofossil zone P11 and planktic foraminiferal zone E4 (formerly
122 P6) [Zachos *et al.*, 2004a, 2004b]. The cores were sampled using a u-channel sampler, and the
123 sediment sliced continuously at 0.5 – 1.0 cm resolution [Stap *et al.*, 2009]. The carbonate content of
124 these samples and bulk carbon and oxygen isotope values were reported by Stap *et al.* [2009].

125 We took a subset of samples for sediment analysis, at 1.0 cm resolution across ETM2 and 10-
126 15 cm pre- and post-event, as defined by [Zachos *et al.*, 2004a, 2004b] (Supporting Information Tables
127 S1 & S2). Samples were washed through a 63 µm sieve using Reverse Osmosis deionised water, dried
128 and split into 63-150 µm and >150 µm size fractions. For benthic foraminiferal analysis a subset of the
129 samples from Stap *et al.* [2009] was used, with a sample spacing of 2.0 cm across ETM2 and 10 cm
130 above and below (Supporting Information Tables S3 & S4).

131 *2.2. Age Model*

132 In the ETM2 age model for Walvis Ridge, Stap and co-workers [Stap *et al.*, 2009] adjusted the
133 terrigenous flux using Gaussian fitting techniques to optimally align the carbon isotope and calcium
134 carbonate weight percent records. The result is an inferred fluctuating terrigenous flux at Site 1262
135 (higher during peak ETM2 conditions) and Site 1265 (lower during peak ETM2 conditions), with
136 stable rates of terrigenous input at Sites 1263 and 1267. Disparity in the sign of terrigenous flux change
137 across the event is somewhat unlikely, given the relative geographic proximity of the sites. Forcing an
138 exact alignment of the primary features of the records is also potentially problematic because the
139 apparent timing of events depends on bulk sediment rate and extent of bioturbation [Ridgwell, 2007], as
140 well as differences in carbonate preservation [Kirtland Turner and Ridgwell, 2013], both of which can
141 be expected to differ between sites and may vary in time.

142 We hence constructed an alternative age model, assuming a stable, site-specific terrigenous flux
143 across the ETM2. There is evidence for generally elevated rates of chemical terrestrial weathering
144 across the PETM (e.g. *Kelly et al.* [2005]; *Ravizza et al.* [2001]) and thus presumably also ETM2, but
145 the total supply rate of particulate terrigenous material to Walvis Ridge may not necessarily have
146 increased. In contrast, if the terrigenous input were dominated by airborne dust, a decrease under global
147 warming would be expected [*Mahowald et al.*, 2006].

148 We calculated relative sediment age based on reported CaCO₃ wt% and dry bulk density [*Zachos et*
149 *al.*, 2004a, 2004b] and using a Terrigenous Mass Accumulation Rate (TMAR) derived from an interval
150 of sedimentation characterized by relatively stable climatic conditions immediately prior to ETM2
151 onset, and between precession cycle tie points of *Westerhold et al.* [2007], at 298.52 – 301.52 mcd at
152 the shallow Site 1263 (~6 x 21 kyr cycles) and 118.5 – 121.83 mcd at the deep Site 1262 (~12 x 21 kyr
153 cycles). The resulting TMARs were 0.154 g/cm²/kyr for Site 1262 and 0.191 g/cm²/kyr at Site 1263. In
154 order to facilitate comparison with previous studies, we calculated Terrigenous Sedimentation Rates
155 (TSRs) for both sites; 0.13 cm/kyr at Site 1263 and 0.12 cm/kyr at Site 1262, and we adopt the zero
156 relative age point defined by [*Stap et al.*, 2009]. Our age model is compared with that in *Stap et al.*,
157 [2009] in Figure 2. A full list of equations can be found in Supporting Information Text S1.

158 2.3. *Sedimentology and benthic foraminiferal analysis*

159 Site-specific bulk and carbonate mass accumulation rates (MAR) were calculated based on our age
160 model. The CaCO₃ fine fraction (FF) (<63 μm) consists predominantly of calcareous nannofossils, the
161 coarse fraction (CF) of planktic foraminifera. We hence used the coarse fraction MAR (> 63 μm)
162 to approximate the foraminiferal mass accumulation rate (FAR). The foraminifera to nannofossil AR
163 was then approximated by dividing the CF AR by the FF AR (>63 μm/<63 μm) (see SI Text S1 for a
164 full equation list). Planktic foraminiferal accumulation rates, in terms of number of specimens
165 (foraminifera #/cm²/kyr), were calculated from planktic foraminiferal counts in the >150 μm size
166 fraction. The effect of dissolution was assessed using fragmentation data [*Le and Shackleton*, 1992],
167 based on counts of five hundred specimens per sample: Fragmentation Ratio (%) = 100% * (Number
168 Fragments/8) / (Number Fragments/8 + Number Whole).

169 We determined the relative abundances of benthic foraminiferal taxa and used these to infer
170 changes in carbonate saturation state, oxygenation and food supply [*Jorissen et al.*, 1995, 2007;
171 *Thomas*, 1998, 2007; *Goody*, 2003; *Goody and Jorissen*, 2012; *Foster et al.*, 2013]. Comparisons

172 between past and recent benthic environments need careful evaluation, because Eocene deep-sea
173 benthic foraminiferal assemblages were structured very differently from today's. For instance, taxa
174 reflecting highly seasonal deposition of organic matter were generally absent or rare, and cylindrically-
175 shaped taxa with complex apertures, which are now extinct, were common (e.g. *Thomas and Gooday*,
176 [1996]; *Thomas*, [2007]; *Hayward et al.*, [2012]). The distribution of these extinct taxa resembles that
177 of buliminids [*Hayward et al.*, 2012], and they were probably infaunal, as confirmed by their $\delta^{13}\text{C}$
178 values [*Mancin et al.*, 2013]. The living species *Nuttallides umbonifera* [*Bremer and Lohmann*, 1982]
179 reaches high relative abundances between lysocline and CCD, and we infer that increases in relative
180 abundance of its ancestral species *N. truempyi* similarly correlate with poorly saturated waters, as
181 confirmed by its bathymetric occurrences [*Thomas*, 1998]. Benthic foraminiferal accumulation rates
182 (BFAR) are a proxy for delivery of food to the sea floor, and generally are higher at shallower depths
183 [*Herguera and Berger*, 1991; *Jorissen et al.*, 2007]. Benthic foraminiferal accumulation rates were
184 calculated as $\text{BFAR} = \text{Benthic foraminifera (\# g}^{-1}\text{)} * \text{Bulk MAR}$. (A full list of sedimentological and
185 derived accumulation rate definitions and calculations is given in Supporting Information Text S1.)

186 2.4. Earth system modelling

187 We explore some of the possible influences on the sediment record of ETM2, including changes in
188 benthic foraminiferal abundance and bioturbation, using the GENIE Earth system model. GENIE
189 comprises a 3D ocean circulation model coupled to a 2D sea-ice and atmospheric energy-moisture-
190 balance-model plus representation of ocean-sediment-weathering carbon cycling, as summarized by
191 *Archer et al.* [2009]. Continental configuration and climatology, initial ocean chemistry, atmospheric
192 CO_2 , and total global weathering flux, are as described by *Ridgwell and Schmidt* [2010]. The model is
193 spun up for a total of 200,000 years to fully balance marine CaCO_3 sedimentation vs. weathering, and
194 create a sufficient sediment column thickness to support any subsequent CaCO_3 'burn-down'
195 [*Ridgwell*, 2007]. The model grid and initial distribution of sedimentary wt% CaCO_3 is illustrated in
196 Figure 1a.

197 To perturb bulk carbonate content and the recording of the $\delta^{13}\text{C}$ signal, the model was run with a
198 prescribed time history of atmospheric composition. We assumed a gradual doubling of $p\text{CO}_2$ over
199 45 kyr from 834 ppm [*Ridgwell and Schmidt*, 2010] to 1668 ppm at the peak of ETM2 [*Stap et al.*,
200 2009], followed by a decline. Atmospheric CO_2 $\delta^{13}\text{C}$ is mirror-imaged and assumes an excursion
201 magnitude of -1.5 ‰ [*Stap et al.*, 2009]. We do not aim to reconstruct the history of CO_2 emissions

202 (unlike e.g. *Kirtland Turner and Ridgwell* [2013]), but instead create and apply to the model a
203 deliberately conceptual time history of atmospheric $p\text{CO}_2$. Doubling of CO_2 in our idealized carbon
204 forcing drives a ~ 2.9 °C warming in mean annual average ocean surface temperatures (~ 3.0 °C in the
205 deep-sea) – consistent with available ETM2 temperature proxies [*Stap et al.*, 2010a; *d’Haenens et al.*,
206 2014]. The form of prescribed $p\text{CO}_2$ and $\delta^{13}\text{C}$ are also chosen such that together, the decline and
207 recovery of $\delta^{13}\text{C}$ can be replicated at Site 1262. Note that we do not attempt to explicitly model $\delta^{18}\text{O}$,
208 which requires a detailed simulation of atmospheric moisture transport and hence a coupled climate
209 model (e.g. *Tindall et al.* [2010]). Given the similarity between $\delta^{13}\text{C}$ and $\delta^{18}\text{O}$ ETM2 horizon
210 anomalies, it is unlikely that simulating $\delta^{18}\text{O}$ in the model would provide additional constraints.

211 To explore what factors might help explain the different sedimentological and isotopic ($\delta^{13}\text{C}$)
212 observations at Site 1263, we ran permutations of: (i) bioturbational mixing occurring continuously
213 throughout the experiment vs. discontinuous bioturbational mixing, with bioturbation ceasing during
214 the peak of the event, (ii) ‘interface’ dissolution of carbonate (the default setting in GENIE) vs.
215 ‘homogeneous’ dissolution [*Ridgwell*, 2001], and (iii) no significant ocean circulation change vs.
216 reduced bottom water saturation at intermediate water depths (which we crudely simulate by increasing
217 the pressure used in calculating carbonate stability at 1263 by the equivalent of 2000 m water depth),
218 summarized in Table 1. All experiments were run for 100 kyr and sediment cores ‘extracted’ from the
219 model grid [*Kirtland Turner and Ridgwell*, 2013; *Ridgwell*, 2007] at locations corresponding to the
220 Walvis Ridge area (Figure 1a) – one at 1500 m model water depth (the model Site 1263 analogue) and
221 one at 3600 m (analogue to 1262). The chronology for the model cores is created analogous to the
222 observations and assumes a constant terrigenous flux to the sediments, which assumes a fixed globally
223 uniform value of $0.180 \text{ g cm}^{-2} \text{ kyr}^{-1}$ following *Panchuk et al.* [2008]. We also ran a 100 kyr long control
224 experiment (‘CTRL’) in which no atmospheric forcing (or modification of bioturbation or local
225 carbonate saturation) was applied.

226

227 3. Results

228 The reconstructed sedimentation rate for both sites is shown in Figure 3, plotted with sediment
229 lightness, alongside core photos [Zachos *et al.*, 2004a, 2004b]. Sedimentation rate at the shallow site
230 was approximately twice the rate at the deep site, with pre-event (< 20 ka) deposition at Site 1263
231 averaging 1.96 cm/kyr, compared with 1.08 cm/kyr at Site 1262. From pre-event to peak-event values,
232 the former sees a ~12-fold drop in sedimentation rate, the latter a 10-fold decrease.

233 As noted but not explained by *Stap et al.*, [2009], bulk stable isotope records for the two sites show
234 clear differences (Figures 2, 4a, b). At the deeper site, bulk $\delta^{13}\text{C}$ values exhibit a gradual decline and
235 then recovery across ETM2. The shallow site, however, also shows a gradual decline/recovery for the
236 start/end of the event, but exhibits an additional excursion during the peak phase (ETM2 horizon; ~38-
237 56 ka). The bulk $\delta^{18}\text{O}$ record similarly shows a greatly enhanced difference within the ETM2 horizon,
238 with much more negative values at the shallow site, although surface dwelling *Acarinina* records do not
239 follow this trend [*Stap et al.*, 2010b]. Intermediate sites along the depth transect, 1265 and 1267 (not
240 shown) are similar to the deep site [*Stap et al.*, 2009].

241 The records of sedimentary CaCO_3 content (Figure 4c) share some features of the bulk stable
242 isotope records [*Stap et al.*, 2009], in as much as the minimum in CaCO_3 wt% at 1263 occurs over a
243 much shorter interval than at 1262, although the minimum CaCO_3 wt% values at both sites are similar.
244 Fragmentation (Figure 4h, Table 2) increased at both sites during ETM2, with the pattern largely
245 mirroring that of CaCO_3 wt% but noisier, with the increase in fragmentation more gradual and longer
246 lasting at the deep site. Similarly, CaCO_3 MAR patterns broadly follow the trend of CaCO_3 content, but
247 the CaCO_3 MAR was higher at the shallow site by a factor of 1.5-2.0 before and after ETM2. Patterns
248 in coarse fraction (i.e., planktic foraminiferal) MAR, susceptible to dissolution and thus indicative of
249 corrosiveness, resemble CaCO_3 MARs, and thus FF MAR, despite its minor contribution to the
250 sediment (Figure 4e, Table 2). Planktic foraminiferal accumulation rates (PFAR – Figure 4g) at both
251 sites were identical prior to the events, but differed during the interval when CaCO_3 wt% remained
252 even at Site 1263, while declining at 1262). The differential changes between the foraminiferal and the
253 coccolithophore response results in relative increases in the foraminiferal contribution to the bulk
254 carbonate at the shallow site between about 16-38 ka (Figure 4f, Table 2), the interval just before the
255 peak of ETM2.

256 Benthic foraminiferal parameters generally resemble sedimentary records. Benthic foraminiferal
257 accumulation rates (BFAR – Figure 5a) at each site were similar before and after the event, with overall

258 slightly higher values at the shallower site. At both sites, BFAR started to decline gradually at the start
259 of ETM2, but more pronouncedly at the deeper site. During start and recovery, the difference in BFAR
260 between the two sites was significantly higher than during background conditions, but during peak
261 ETM2 (40-55 ka) BFAR values at Site 1263 declined precipitously, below those at Site 1262 (Figure
262 5a; Table 4). Samples were essentially barren of benthic foraminifera [Stap *et al.*, 2010b]. All species-
263 specific ARs declined (Supporting Information Figure S1, Table 5). No species bloomed during ETM2:
264 all declined in abundance, though some more than others. The diversity (rarefied number of species)
265 declined parallel to BFAR, with largest differences between the sites during the start (and recovery)
266 phase when values at the shallower site remained relatively high while those at the deep site had started
267 to decline (and had not yet recovered) (Table 4).

268 Benthic foraminiferal assemblages during background conditions were diverse, with 133 taxa
269 recognized, 117 at the deep site (18 not present at 1263), 116 at Site 1263 (17 not present at Site 1262)
270 (Supplementary Information Data Set S1). The number of species (rarefied to 100 specimens) was
271 higher at the shallow site (background values of 41 species) than at the deep site (33 species)
272 (Figure 5b), largely due to the presence of diverse species of *Lenticulina* and other lagenid species.
273 *Nuttallides truempyi* was the most common species at both sites, with *Oridorsalis umbonatus*,
274 *Quadriformina profunda*, *Bulimina kugleri*, and *Bulimina simplex* (Table 3). Species present at the
275 shallow site only include *Cibicidoides alleni* and *C. laurisaе* and the agglutinant *Vulvulina jarvisae*, as
276 well as several uniserial lagenid species. Those present at the deep site only include mainly agglutinant
277 species (e.g. *Repmanina charoides*, *Trochamminoides serpens*, *Siphotextularia rolszhauseni*). All
278 species present at one site only are rare (< 0.5 of total assemblage).

279 During ETM2, *Nuttallides truempyi* and *N. umbonifera* increased in relative abundance (Figure 5c)
280 at the deep site, as did *Abyssamina poagi*, *Globocassidulina subglobosa* and *Cibicidoides* species,
281 whereas *Tappanina selmensis* and *Siphogenerinoides brevispinosa*, probably opportunistic infaunal
282 taxa [Steineck and Thomas, 1996; Thomas, 1998, 2003], decreased in relative abundance (Figure 5d, f,
283 g). Epifaunal species thus overall increased in relative abundance at the deep site and infaunal species
284 decreased (Figure 5e) during the full duration of ETM2. In contrast, at the shallow site, infaunal taxa as
285 a whole, and the generally infaunal buliminid and cylindrical species remained equal or increased
286 somewhat in relative abundance during the start of ETM2, so that the difference in relative abundances
287 at the two sites increased (Figure 5e, h, i). A similar difference developed during the recovery phase. In
288 addition, the shallow infaunal *Oridorsalis umbonatus* [Thomas and Shackleton, 1996] increased in
289 relative abundance at the shallow site just after the peak event (Figure 5j). During the peak event

290 benthic foraminifera were essentially absent at Site 1263. After the peak event and extending after the
291 recovery phase, agglutinant taxa at the deep site remained less abundant, as did *Siphogenerinoides*
292 *brevispinosa*. *Epistominella exigua* became more common after ETM2, and *Quadrinorphina profunda*
293 did so at the shallow site (e.g. Figure 5g, k).

294

295 4. Discussion

296 The biotic and sedimentary records across ETM2 at Walvis Ridge are striking in their similarity. Both
297 record more gradual change at the deeper site, with a generally more extreme and much shorter
298 superimposed change during the peak of the event at the shallower site only. If CO₂ addition and
299 associated decline in carbonate saturation alone were driving the sedimentary observations, we would
300 have expected a sharper wt% CaCO₃ response at 1262 compared to 1263 because of the lower initial
301 saturation and hence lower fractional carbonate preservation at greater depth [Stap *et al.*, 2009].
302 Assuming a similar ocean acidification (carbonate ion decline) at all depths, the non-linear nature of the
303 wt% CaCO₃ scale means that at lower initial wt% CaCO₃, only a relatively small decline in carbonate
304 preservation is needed to produce a large change in wt%. Instead, we observe the opposite, i.e., a
305 sharper response at the shallow site, which starts at higher wt% CaCO₃. There is no indication of
306 unconformities (Figure 3) [Stap *et al.*, 2009] bracketing the ETM2 horizon and hence no indication of a
307 removal of most of the onset and recovery at Site 1263 to explain the sharp transitions. We also discard
308 the possibility of sampling biases. Stap *et al.* [2009] sampled 1262 more closely spaced (at 0.5 cm)
309 within the ETM2 horizon. Hence wt% CaCO₃, $\delta^{13}\text{C}$, and $\delta^{18}\text{O}$ (Figure 4 a-c) measurements are more
310 closely spaced in time at the deep site, implying that the smoother bulk carbonate composition trends at
311 1262 cannot be due to a sampling artefact. If anything, the less frequent sampling in depth (thus time)
312 across the ETM2 horizon at 1263 could have underestimated the abruptness of the transition into and
313 out of peak ETM2 conditions. We also rule out sampling differences as an explanation for the absence
314 of benthic foraminifera at 1263. Unlike the bulk carbonate records, sampling for benthic foraminiferal
315 analysis was regular (2 cm). The difference in sedimentation rates, which prior to ETM2 averaged
316 1.08 cm/kyr at the deep site compared with 1.96 cm/kyr at the shallow site hence leads to a higher
317 frequency in time of sampling at 1263 vs. 1262. It is extremely unlikely that the presence of
318 foraminifera during the ETM2 horizon was missed in the more frequently sampled (in time) core.

319 4.1. Benthic foraminiferal response to the ETM2

320 In general, the most diverse benthic assemblages, with co-occurring epifaunal and infaunal dwellers,
321 are indicative of intermediate food availability. When little particulate organic carbon arrives at the
322 seafloor, there is insufficient food to sustain infaunal populations, and at extreme food abundance,
323 oxygen levels in pore waters (and finally in bottom waters) become too low to sustain infaunal

324 populations [Jorissen *et al.*, 2007]. The relative abundance of infaunal taxa thus is a proxy for
325 increased food supply and/or declining oxygen levels.

326 At the deep site, BFAR as well as relative abundance of infaunal taxa (buliminids, cylindrical taxa)
327 declined gradually to reach the lowest levels for that site during the peak event, before increasing again
328 (Figure 5; Table 4). Relative abundances of *N. truempyi* and *N. umbonifera*, indicative of
329 undersaturated bottom waters and/or oligotrophic conditions [Bremer and Lohmann, 1982; Thomas,
330 1998] increased, as did that of the abyssaminids. The latter are extinct, but were generally more
331 abundant at greater depths (e.g., Thomas, [1998]), thus probably indicative of oligotrophic conditions.
332 All benthic foraminiferal indicators point to a declining food supply to the seafloor during ETM2 at
333 Site 1262. In contrast, calcareous nannofossil evidence for nearby Site 1265 does not indicate
334 significant changes in productivity in the region [Dedert *et al.*, 2012].

335 Can indicators of relatively unchanging surface productivity be reconciled with an interpretation of
336 declining benthic food supply? It is unlikely that the strong decrease in BFAR and diversity is driven
337 by taphonomic dissolution only, because the proportion of *Abyssamina poagi*, a small, smooth,
338 dissolution-prone taxon, increased during peak ETM2, i.e. maximum dissolution (Figure 5c), whereas
339 dissolution would have led to a relative increase in relatively large, heavily calcified taxa (e.g., *Nguyen*
340 *et al.*, [2009], *Nguyen and Speijer*, [2014]). Instead, we suggest that temperature changes associated
341 with ETM2 are key. Higher temperatures influence biological processes [Pörtner *et al.*, 2014] due to
342 their effect on enzyme reactions, diffusion and membrane transport [Hochachka and Somero, 2002],
343 increasing metabolic rates [Hoegh-Guldberg and Bruno, 2010]. Temperature-driven increased
344 metabolic rates at a constant food supply would by themselves produce an energy deficit. In addition,
345 warmer oceans might see a greater degree of remineralization of organic matter in the water column
346 [O'Connor *et al.*, 2009], a possibility e.g. demonstrated for the Eocene of off-shore Tanzania on the
347 basis of reconstructed water column $\delta^{13}\text{C}$ gradients [John *et al.*, 2014]. Increased metabolic rates
348 combined with increased remineralization of organic matter in the water column leads to a lesser
349 arrival of food at the seafloor despite constant productivity [Ma *et al.*, 2014], and could, coupled with
350 the highly food-limited nature of benthic foraminifera in today's oceans [Linke, 1992], explain the
351 strongly reduced BFARs.

352 Faunal changes were more complex at the shallower site, despite the fact that the sites are relatively
353 close to each other and hence under waters with similar primary productivity [Zachos *et al.*, 2004a,
354 2004b]. Whereas BFAR, species diversity and buliminid taxa all decreased simultaneously during the

355 early and recovery phase of ETM2 at the deep site, the relative abundance of buliminid taxa at the
356 shallow site increased, despite decreasing BFAR and species diversity (Figure 5). Several infaunal taxa
357 decreased in relative abundance at Site 1263 during the peak-ETM2 (e.g., *S. brevispinosa* and *T.*
358 *selmensis* Figs 5f, g) suggesting that these taxa were less able to survive the lowered food supply at this
359 site, indicated by the more severe drop in BFAR, than other infaunal taxa such as buliminids. In
360 contrast these species decline similarly to buliminids at Site 1262. During the recovery phase, the
361 relative abundance of the shallow infaunal *O. umbonatus* increased; this increase was likely not caused
362 by an increase in food supply, because the BFAR remained low relative to pre-event values. Buliminid
363 taxa and *O. umbonatus* % increased in relative abundance just prior to the peak-event (20 – 40 kyr).
364 Both calcify in the less saturated pore waters rather than in bottom waters, so the increase might have
365 been caused by increasing undersaturation [Foster *et al.*, 2013], but this does not agree with the
366 observation that at the shallow site the carbonate parameters (CaCO₃ wt %, fragmentation, PFAR)
367 remained constant during the interval with increased abundance of buliminid taxa. This increased
368 abundance of buliminid taxa and *O. umbonatus* during declining food levels and invariant carbonate
369 corrosiveness thus indicates that oxygenation was declining in bottom and/or pore waters at the shallow
370 site, possibly due to rising temperatures, increased remineralisation of organic matter or changes in pre-
371 formed oxygen levels due to changes in ocean circulation pattern.

372 During the peak phase of ETM2, benthic foraminifera were absent at Site 1263, indicating that
373 bottom and pore water conditions could not support them, and were less favourable than at the deeper
374 Site 1262 where benthic foraminifera remained present. Deoxygenation was more severe and persisted
375 longer at the sea floor at Site 1263 than at Site 1262 during the PETM at the Walvis Ridge based on
376 bulk sediment trace element data [Chun *et al.*, 2010; Pälike *et al.*, 2014] and mineralogical data [Post *et*
377 *al.*, 2015]. A similar occurrence during ETM2 would help explain the differential benthic assemblage
378 changes between Sites 1262 and 1263. Benthic foraminiferal records during the PETM cannot be
379 compared between the sites because of the severe carbonate dissolution during the peak PETM, with
380 CaCO₃ fully dissolved for part of the PETM at all sites, longer at the deeper sites [Zachos *et al.*, 2005].

381 4.2. Ocean circulation as a driver of depth-specific ecological change

382 We interpret our observations in terms of a change in the source of intermediate waters bathing Site
383 1263, driving a much larger warming and decrease in dissolved oxygen compared to 1262. Support for
384 this comes from the results of Paleocene / early Eocene fully coupled atmosphere-ocean climate

385 general circulation model experiments [Lunt *et al.*, 2010]. These experiments demonstrate that an
386 atmospheric CO₂ and surface warming threshold could exist, beyond which any further CO₂ rise and
387 surface warming leads to a disproportionately larger increase in temperature increase in the
388 intermediate waters than in the deep ocean. For instance, in the simulations of Lunt *et al.* [2010], going
389 from 2 x PAL to 6 x PAL CO₂, where PAL is 280 ppmv, produced a warming of 1.7 °C at 1500 m
390 compared to 0.2 °C at ~3500 m (Figure 6). All other things being equal, a change in water mass source
391 and/or mixing that leads to higher local temperatures will be associated with lower dissolved O₂,
392 although the specific pathway and hence integrated remineralization of organic matter along that
393 pathway will also affect the local value of [O₂].

394 A change in circulation during ETM2 has also been suggested by *d'Haenens et al.* [2014], inferred
395 from a short-lived reversal of meridional δ¹³C gradients of 0.50 – 1.00 ‰ between the north and south
396 Atlantic (DSDP Sites 401 and 550, NE Atlantic and the Walvis Ridge sites respectively). Similarly
397 ocean circulation change has been inferred at Site 1263 during the PETM as implied by the largest CIE
398 (–3.5 ‰) in deep-sea benthics, though comparison with the other sites is not possible due to the severe
399 dissolution [McCarren *et al.*, 2008]. Direct evidence for a circulation change driven warming does not
400 yet exist however. Although a 3 °C warming during ETM2 was estimated from benthic foraminifera at
401 1262 [Stap *et al.*, 2010a], the relative temperature change at the shallower site is not recorded due to
402 the absence of benthic foraminifera during the critical interval.

403 4.3. *Origins of the 'anomalous' bulk sediment response during peak ETM2 conditions*

404 We suggest that the Site 1263 phenomena: (1) a sharp excursion in wt% CaCO₃ together with bulk
405 carbonate δ¹³C and δ¹⁸O that constitutes the ETM2 horizon; and (2) temporary exclusion of benthic
406 foraminifera are causally linked, via the impact of changes in the benthic foraminiferal contribution to
407 bioturbation [Grosse, 2002]. We infer that sediment mixing by benthic foraminifera would have
408 effectively ceased at the shallow site during the peak of ETM2. Changes in bottom water conditions
409 would have also affected other benthic biota (including burrowers) because animals are more severely
410 affected by deoxygenation than protists such as foraminifera [Goody *et al.*, 2010]. Surface sediment
411 mixing thus may have ceased during the peak of ETM2 at the shallow site, but not at the deep site, as
412 may be seen in the core photographs, and in the larger and more abrupt change in sediment color
413 (lightness) (Figure 3). This is important, as mixing reduces the recorded magnitude and increases the
414 apparent duration of a signal [Ridgwell, 2007; Kirtland Turner and Ridgwell, 2013]. Indeed, numerical

415 modelling of hyperthermal events illustrates that a sharper onset to low carbonate content sediments is
416 observed in the absence of bioturbation [Ridgwell, 2007; Kirtland Turner and Ridgwell, 2013]. An
417 enhanced degree of carbonate dissolution in the ETM2 horizon at 1263 might also have played a role,
418 as the temporary emplacement of a less well ventilated intermediate water mass would be expected to
419 have higher respired dissolved CO₂ concentrations and hence lower saturation. We turn to the Earth
420 system modelling experiments (Table 1) to explore this further.

421 We first test whether the assumed atmospheric perturbation (Figure 7a) can produce a sediment
422 record consistent with observations from the deep site, where we expect a relatively straightforward
423 and predictable response to ETM2 ocean acidification. In experiment ‘STD’ (Table 1), we simulate a
424 reduction in carbonate content to around 50 wt% in response to increasing atmospheric CO₂ followed
425 by an initially more rapid recovery (Figure 5b), qualitatively consistent with trends observed at Site
426 1262. Towards the end of the simulation, the modelled sediment record displays an ‘overshoot’ in
427 carbonate content which is also expected [Dickens *et al.*, 1997; Zachos *et al.*, 2005; Kump *et al.*, 2009]
428 although in this specific model example it occurs due to a forced removal of CO₂ from the atmosphere
429 (Figure 7a) rather than via an explicit calculation of silicate weathering feedback [Colbourn *et al.*,
430 2013]. Carbonate δ¹³C (Figure 5b) exhibits an excursion size slightly less than the applied -1.5 ‰
431 magnitude of the forcing (Figure 5a), also as expected [Kirtland Turner and Ridgwell, 2013]. However,
432 the δ¹³C minimum lags that of wt % CaCO₃ by about 10 kyr, whereas in the Site 1262 observations
433 (Figure 4 a & c) they are approximately synchronous. In experiment ‘ALT’ we hence substitute a
434 ‘homogeneous’ carbonate dissolution model for the default ‘interface’ assumption [Ridgwell, 2001], so
435 that newly deposited carbonate is mixed into the surface sediment layer before carbonate is removed
436 through dissolution. This brings the δ¹³C and wt % CaCO₃ minima into alignment (Figure 7c),
437 producing a better match to the Site 1262 observations. (In the ‘interface’ model of carbonate
438 dissolution, a δ¹³C signal from the surface cannot be imprinted on the sediments once the total
439 dissolution flux exceeds the rain flux.) However, little change in wt % CaCO₃ is recorded at the
440 analogue location to Site 1263 (Figure 7d). In addition, the simulated δ¹³C record at 1263 is too regular,
441 and exhibits none of the abrupt transitions characterizing the observed transition into and out of the
442 ETM2 horizon (Figure 3, 4). In experiments: ‘ALT_bio’, ‘ALT_sat’, and ‘ALT_satbio’, we hence
443 explore the possible impact of reduced carbonate saturation, reduced bioturbation, and both together
444 (Table 1).

445 The temporary cessation of sediment mixing on its own (‘ALT_bio’) at 1263 does little more than

446 introduce small step-like features in the simulated evolution of bulk carbonate $\delta^{13}\text{C}$ (Figure 7d), with
447 little noticeable impact on wt % CaCO_3 . In contrast, temporarily decreasing carbonate saturation on its
448 own ('ALT_sat') reduces wt % CaCO_3 towards observed Site 1262 values (Figure 7c, f). The
449 transitions in bulk composition occur relatively rapidly, to create a simulated feature more reminiscent
450 of the ETM2 horizon (Figure 4c). Combining both temporary saturation decline and cessation of
451 bioturbation ('ALT_satbio') leads to a more sharply defined wt % CaCO_3 anomaly, particularly with
452 respect to the transition into the peak of the event (Figure 7g). However, only small steps occur in $\delta^{13}\text{C}$.

453 Although not successful in reproducing all the observations, these simple experiments reveal the
454 potential processes associated with specific sedimentary features. First, we find that a change in water
455 mass saturation appears to be key to reproducing the magnitude of anomalous decline and recovery in
456 wt % CaCO_3 at Site 1263. That said, we cannot rule out the possibility that the GENIE model does not
457 exhibit an appropriate sensitivity of carbonate preservation to CO_2 addition, particularly as a function
458 of ocean depth. Although outside the scope of this particular paper, the model response to ETM2 could
459 be assessed by contrasting the changes in CaCO_3 across the event (Figure 1a, b) at multiple sites
460 spanning different ocean basins (e.g., as in *Panchuk et al.* [2008]) and the applied forcing refined,
461 perhaps by means of formal inversion [*Kirtland Turner and Ridgwell, 2013*]. In contrast to reduced
462 saturation, the importance of bioturbation is apparent in dictating the details of the recorded shape of
463 the signal. Only by stopping mixing (bioturbation) between model sediment layers can a sharp decline
464 at the onset of the ETM2 horizon be reproduced. In our model (experiments 'ALT_bio' and
465 'ALT_satbio') bioturbation is switched fully back on at 65 ka, and the consequential transition in wt %
466 CaCO_3 is comparatively gradual. The BFAR record (Figure 5a) suggests a more drawn-out recovery of
467 the benthos and attendant gradual increase in the intensity of bioturbation. If implemented in the model,
468 we would expect a sharper transition at the end of the ETM2 horizon, closer to observations.

469 If the above analysis is correct and the attributes of the ETM2 horizon at Site 1263 are primarily
470 driven by a local circulation change and its associated benthic ecological impact, this creates a
471 challenge for understanding when these additional effects occurred relative to the primarily CO_2 -driven
472 carbonate dissolution at greater depth. In our age model, we adopt the same tie-point as *Stap et al.*
473 [2009] to define the start of ETM2 (0 ka in e.g., Figure 2). This places the required circulation change
474 at Site 1263 approximately coincident with peak ETM2 conditions at 1262. If we shifted the record for
475 1263 older by one precession cycle instead, the circulation change would occur close to the ETM2
476 onset at 1262. This would be a plausible alternative alignment, particularly if the carbon release were

477 rapid.

478 Finally, our failure to explain the full magnitude of observed $\delta^{13}\text{C}$ changes at Site 1263 (and not
479 explored here in the model – also of $\delta^{18}\text{O}$) is more difficult to account for. We thus do not rule out that
480 differential dissolution or diagenetic alteration might explain some of the observed disparity in bulk
481 carbonate proxy responses between sites. However, the carbon isotope signals in marine carbonate are
482 generally thought to not be significantly affected by diagenesis [Sexton *et al.*, 2006] and burial depth
483 [Schrag *et al.*, 1995]. Furthermore, differences between the bulk $\delta^{13}\text{C}$ values at the two sites are not
484 likely caused by differences in the nanoplankton assemblage composition, because vital effects are
485 minor [Ziveri *et al.*, 2003] and assemblages at the sites similar [Agnini *et al.*, 2007; Raffi and De
486 Bernardi, 2008; Dedert *et al.*, 2012]. Although there is some variation in the relative proportions of the
487 CF (foraminifera) and FF (nanoplankton) during the ETM2, the ratio continues to be dominated by
488 calcareous nannofossils (Figure 4d). For $\delta^{18}\text{O}$, recrystallization [Schrag *et al.*, 1995] could potentially
489 imprint a component of bottom water temperature at Site 1263, but this would imply that the 1262
490 record reflects extensive recrystallization because of the lower bottom water temperatures at that site.
491 This seems rather unlikely as burial depths were on the order of 100 m only at Site 1262, i.e. much less
492 than the >300 m at Site 1263, and recrystallization should have been much less pronounced at the
493 deeper site [Zachos *et al.*, 2004a]. None of these diagenetic-based explanations are thus particularly
494 compelling.

495

496

497 **5. Conclusions**

498 During the ETM2, Walvis Ridge Sites 1263 and 1262 both record a $\delta^{13}\text{C}$ excursion, warming, and
499 evidence of ocean acidification. The benthic foraminiferal ecosystem was perturbed in response to
500 environmental change during the ETM2, with a decrease in abundance, diversity and assemblage
501 change at both sites. However, a more severe benthic response occurred at the shallow site, resulting in
502 the temporary absence of benthic foraminifers. We infer that this was caused by more pronounced
503 intermediate water warming, leading to effective decline in food supply and deoxygenation driven by a
504 circulation change. This in turn led to a cessation of bioturbation and a possible accentuation of the
505 sedimentological record of the event at 1263. We used a simple conceptual carbon forcing model for a
506 temporary cessation of sediment mixing plus a decrease in carbonate saturation associated with
507 changing intermediate water mass properties. Using this model, we can qualitatively account for the
508 bulk sediment and carbon isotopic observations at both sites. However, a full explanation for the
509 greater magnitude of recorded isotopic excursion at Site 1263 remains to be identified. Our study
510 illustrates that the biotic response to a global change event can be highly spatially heterogeneous and
511 not necessarily scale simply with the magnitude of the event. Instead, the effects of increased
512 atmospheric CO_2 can lead to ocean circulation change and other feedbacks that create a far more
513 complex picture of the influence of climate change on biota. In turn, changes in biota can distort the
514 sedimentary proxy record.

515

516 **Acknowledgments**

517 This work was supported by a Royal Society University Research Fellowship awarded each to A.
518 Ridgwell and D Schmidt, and NERC grant NE/H023852/1 (to A. Ridgwell and D. Schmidt). E.
519 Thomas was supported by the Leverhulme Trust and NSF Grants OCE-0903014 and OCE-1232413.

520 S. Jennions was supported by a donation through the University of Bristol Alumni Foundation - special
521 thanks to two benefactors who have made this research possible. Data is available at Pangaea,
522 <http://doi.pangaea.de/10.1594/PANGAEA.845418>.

523

524

525 **REFERENCES**

- 526 Abels, H.A., W. C. Clyde, P. D. Gingerich, F. J. Hilgen, H. C. Fricke, G. J. Bowen, and L. J. Lourens
527 (2012), Terrestrial carbon isotope excursions and biotic change during Palaeogene hyperthermals,
528 *Nature Geoscience*, 5(5), 326–329.
- 529 Agnini, C., E. Fornaciari, D. Rio, F. Tateo, J. Backman, and L. Giusberti (2007), Responses of
530 calcareous nannofossil assemblages, mineralogy and geochemistry to the environmental
531 perturbations across the Paleocene/Eocene boundary in the Venetian Pre-Alps, *Marine*
532 *Micropaleontology*, 63(1), 19-38.
- 533 Agnini, C., P. Macrì, J. Backman, H. Brinkhuis, E. Fornaciari, L. Giusberti, V. Luciani, D. Rio, A.
534 Sluijs, and F. Speranza (2009), An early Eocene carbon cycle perturbation at ~52.5 Ma in the
535 Southern Alps: Chronology and biotic response, *Paleoceanography*, 24(2), 1–14.
- 536 Alegret, L., S. Ortiz, I. Arenillas, and E. Molina (2010), What happens when the ocean is overheated?
537 The foraminiferal response across the Paleocene-Eocene Thermal Maximum at the Alamedilla
538 section (Spain), *Geological Society of America Bulletin*. 122(9-10), 1616–1624.
- 539 Archer, D., M. Eby, V. Brovkin, A. Ridgwell, L. Cao, U. Mikolajewicz, K. Caldeira, K. Matsumoto, G.
540 Munhoven, A. Montenegro and K. Tokos. (2009). Atmospheric lifetime of fossil fuel carbon
541 dioxide. *Annual Review of Earth and Planetary Sciences*, 37(1), 117.
- 542 Bopp, L., L. Resplandy, J. C. Orr, S. C. Doney, J. P. Dunne, M. Gehlen, ... and M. Vichi, (2013).
543 Multiple stressors of ocean ecosystems in the 21st century: projections with CMIP5
544 models. *Biogeosciences*, 10, 6225-6245.
- 545 Bralower, T. J. (2002), Evidence of surface water oligotrophy during the Paleocene-Eocene thermal
546 maximum : Nannofossil assemblage data from Ocean Drilling Program Site 690, Maud Rise,
547 Weddell Sea, *Paleoceanography*, 17(2), 13-1.
- 548 Bremer, M., and G. Lohmann (1982), Evidence for primary control of the distribution of certain
549 Atlantic Ocean benthonic foraminifera by degree of carbonate saturation, *Deep Sea Research Part*
550 *A. Oceanographic Research Papers*, 29(8), 987-998.
- 551 Caldeira, K., & M. E. Wickett, (2003). Oceanography: anthropogenic carbon and ocean
552 pH. *Nature*, 425(6956), 365-365.
- 553 Chun, C. O. J., M. L. Delaney, and J. C. Zachos (2010), Paleo-redox changes across the Paleocene-
554 Eocene Thermal Maximum, Walvis Ridge (ODP Sites 1262, 1263, and 1266): Evidence from Mn
555 and U enrichment factors, *Paleoceanography*, 25(4).
- 556 Clementz, M., S. Bajpai, V. Ravikant, J. G. M. Thewissen, N. Saravanan, I. B. Singh, and V. Prasad
557 (2011), Early Eocene warming events and the timing of terrestrial faunal exchange between India
558 and Asia, *Geology*, 39(1), 15–18.

- 559 Colbourn, G., A. Ridgwell, and T. M. Lenton, (2013). The Rock Geochemical Model (RokGeM) v0.
560 9. *Geoscientific Model Development*, 6(5), 1543-1573.
- 561 Coma, R., M. Ribes, E. Serrano, E. Jiménez, J. Salat and J. Pascual, (2009). Global warming-enhanced
562 stratification and mass mortality events in the Mediterranean. *Proceedings of the National*
563 *Academy of Sciences*, 106(15), 6176-6181.
- 564 Cramer, B. S., Wright, J. D., Kent, D. V., and M. P. Aubry (2003). Orbital climate forcing of $\delta^{13}\text{C}$
565 excursions in the late Paleocene–early Eocene (chrons C24n–C25n). *Paleoceanography*, 18(4) 1-
566 25.
- 567 Crouch, E. M., C. Heilmann-Clausen, H. Brinkhuis, H. E. Morgans, K. M. Rogers, H. Egger, and B.
568 Schmitz, (2001), Global dinoflagellate event associated with the late Paleocene thermal maximum,
569 *Geology*, 29(4), 315–318.
- 570 d’Haenens, S., A. Bornemann, P. Stassen, and R. P. Speijer (2012), Multiple early Eocene benthic
571 foraminiferal assemblage and $\delta^{13}\text{C}$ fluctuations at DSDP Site 401 (Bay of Biscay — NE
572 Atlantic), *Marine Micropaleontology*, 88, 15–35.
- 573 d’Haenens, S., A. Bornemann, P. Claeys, U. Röhl, E. Steurbaut, and R. P. Speijer (2014), A transient
574 deep-sea circulation switch during Eocene Thermal Maximum 2 (ETM2), *Paleoceanography*,
575 29(5), 370-388.
- 576 Dedert, M., H. M. Stoll, D. Kroon, N. Shimizu, K. Kanamaru, and P. Ziveri (2012), Productivity
577 response of calcareous nannoplankton to Eocene Thermal Maximum 2 (ETM2), *Climate of the*
578 *Past*, 8(3), 977–993.
- 579 Dickens, G. R., M. M. Castillo, and J. C. Walker (1997), A blast of gas in the latest Paleocene:
580 simulating first-order effects of massive dissociation of oceanic methane hydrate., *Geology*, 25(3),
581 259–62.
- 582 Dunkley Jones, T., D. J. Lunt, D. N. Schmidt, A. Ridgwell, A. Sluijs, P. J. Valdes, and M. Maslin
583 (2013), Climate model and proxy data constraints on ocean warming across the Paleocene–Eocene
584 Thermal Maximum, *Earth-Science Rev.*, 125, 123–145.
- 585 Durack, P. J., S. E. Wijffels, and R. J. Matear, (2012). Ocean salinities reveal strong global water cycle
586 intensification during 1950 to 2000. *Science*, 336(6080), 455-458.
- 587 Foster, L. C., D. N. Schmidt, E. Thomas, S. Arndt, and A. Ridgwell (2013), Surviving rapid climate
588 change in the deep sea during the Paleogene hyperthermals., *Proc. Natl. Acad. Sci. U. S. A.*,
589 110(23), 1–4.
- 590 Gibbs, S. J., T. J. Bralower, P. R. Bown, J. C. Zachos, and L. M. Bybell (2006), Shelf and open-ocean
591 calcareous phytoplankton assemblages across the Paleocene-Eocene Thermal Maximum:
592 Implications for global productivity gradients, *Geology*, 34(4), 233.

- 593 Gooday, A. (2003), Benthic foraminifera (Protista) as tools in deep-water palaeoceanography:
594 environmental influences on faunal characteristics, *Advances in Marine Biology*, 46, 1-90.
- 595 Gooday, A. J., and F. J. Jorissen (2012), Benthic Foraminiferal Biogeography: Controls on Global
596 Distribution Patterns in Deep-Water Settings, *Ann. Rev. Mar. Sci.*, 4(1), 237–262.
- 597 Gooday, A. J., B. J. Bett, E. Escobar, B. Ingole, L. A. Levin, C. Neira, A. V. Raman, and J. Sellanes
598 (2010), Habitat heterogeneity and its influence on benthic biodiversity in oxygen minimum zones,
599 *Marine Ecology.*, 31(1), 125–147.
- 600 Grosse, O. (2002), Sediment interactions of foraminifera: Implications for food degradation and
601 bioturbation processes, *The Journal of Foraminiferal Research*, 32(4), 414–424.
- 602 Hayward, B. W., S. Kawagata, A. T. Sabaa, H. R. Grenfell, L. van Kerckhoven, K. Johnson, and E.
603 Thomas (2012), The Last Global Extinction (Mid-Pleistocene) of Deep-Sea Benthic Foraminifera
604 (Chrysalogoniidae, Ellipsoidinidae, Glandulonodosariidae, Plectofrondiculariidae,
605 Pleurostomellidae, Stilostomellidae), their Late Cretaceous-Cenozoic History and Taxonomy.,
606 *Cushman Found. Foraminifer. Res. Spec. Vol.*, 43, 408.
- 607 Herguera, J., and W. Berger (1991), Paleoproductivity from benthic foraminifera abundance: Glacial to
608 postglacial change in the west-equatorial Pacific, *Geology* 19(12), 1173-1176.
- 609 Hochachka, P. W., and G. N. Somero (2002), *Biochemical adaptation: mechanism and process in*
610 *physiological evolution*, 480th ed., New York: Oxford University Press.
- 611 Hoegh-Guldberg, O., and J. F. Bruno (2010), The impact of climate change on the world's marine
612 ecosystems., *Science*, 328(5985), 1523–8.
- 613 Hollis, C. J. (2006), Radiolarian faunal turnover through the Paleocene-Eocene transition, Mead
614 Stream, New Zealand, *In Radiolaria (pp. 79-99). Birkhäuser Basel*.
- 615 Hönisch, B., A. Ridgwell, D. N. Schmidt, E. Thomas, S. J. Gibbs, A. Sluijs, ... & B. Williams. (2012),
616 The Geological Record of Ocean Acidification, *Science*, 335(6072), 1058–1063.
- 617 Hutchins, D. A., F.-X. Fu, Y. Zhang, M. E. Warner, Y. Feng, K. Portune, P. W. Bernhardt, and M. R.
618 Mulholland (2007), CO₂ Control of Trichodesmium N₂ Fixation, Photosynthesis, Growth Rates,
619 and Elemental Ratios: Implications for Past, Present, and Future Ocean Biogeochemistry. *Limnol.*
620 *Oceanogr.*, 52(4), 1293–1304.
- 621 John, E. H., J. D. Wilson, P. N. Pearson and A. Ridgwell, (2014). Temperature-dependent
622 remineralization and carbon cycling in the warm Eocene oceans, *Palaeogeography,*
623 *Palaeoclimatology, Palaeoecology*, 413, 158-166.
- 624 Jorissen, F. J., H. C. de Stigter, and J. G. V. Widmark (1995), A conceptual model explaining benthic
625 foraminiferal microhabitats, *Mar. Micropaleontol.*, 26(1-4), 3–15.

- 626 Jorissen, F., C. Fontanier, and E. Thomas (2007), Paleooceanographical proxies based on deep-sea
627 benthic foraminiferal assemblage characteristics. In: Proxies in Late Cenozoic Paleooceanography:
628 Pt. 2: Biological tracers and biomarkers, edited by C. Hillaire-Marcel and A. de Vernal, Elsevier,
629 p. 263-326.
- 630 Keeling, R. F., A. Körtzinger, and N. Gruber (2010), Ocean Deoxygenation in a Warming World,
631 *Annual review of marine science*, 2(1), 199–229.
- 632 Kelly, D. C., T. J. Bralower, J. C. Zachos, I. P. Silva, and U. Milano (1996), Rapid diversification of
633 planktonic foraminifera in the tropical Pacific (ODP Site 865) during the late Paleocene thermal
634 maximum, *Geology*, 24, 423–426.
- 635 Kelly, D. C., J. C. Zachos, T. J. Bralower, and S. A. Schellenberg, (2005). Enhanced terrestrial
636 weathering/runoff and surface ocean carbonate production during the recovery stages of the
637 Paleocene-Eocene thermal maximum. *Paleoceanography*, 20(4).
- 638 Kirtland Turner, S., and A. Ridgwell (2013), Recovering the true size of an Eocene hyperthermal from
639 the marine sedimentary record, *Paleoceanography*, 28(4), 700-712.
- 640 Kump, L., T. Bralower, and A. Ridgwell (2009), Ocean acidification in deep time, *Oceanography*,
641 22(4), 94–107.
- 642 Le, J., and N. Shackleton (1992), Carbonate dissolution fluctuations in the western equatorial Pacific
643 during the late Quaternary, *Paleoceanography*, 7(1), 21–42.
- 644 Linke, P. (1992), Metabolic adaptations of deep-sea benthic foraminifera to seasonally varying food
645 input., *Mar. Ecol. Prog. Ser. Oldendorf*, 81, 51–63.
- 646 Littler, K., U. Röhl, T. Westerhold, and J. C. Zachos (2014), A high-resolution benthic stable-isotope
647 record for the South Atlantic: Implications for orbital-scale changes in Late Paleocene-Early
648 Eocene climate and carbon cycling, *Earth Planet. Sci. Lett.*, 401, 18–30.
- 649 Lourens, L. J., A. Sluijs, D. Kroon, J. C. Zachos, E. Thomas, U. Röhl, J. Bowles, and I. Raffi (2005),
650 Astronomical pacing of late Palaeocene to early Eocene global warming events., *Nature*,
651 435(7045), 1083–7.
- 652 Luciani, V., L. Giusberti, C. Agnini, J. Backman, E. Fornaciari, and D. Rio (2007), The Paleocene–
653 Eocene Thermal Maximum as recorded by Tethyan planktonic foraminifera in the Forada section
654 (northern Italy), *Mar. Micropaleontol.*, 64(3-4), 189–214.
- 655 Lunt, D. J., P. J. Valdes, T. D. Jones, A. Ridgwell, A. M. Haywood, D. N. Schmidt, R. Marsh, and M.
656 Maslin (2010), CO₂-driven ocean circulation changes as an amplifier of Paleocene-Eocene
657 thermal maximum hydrate destabilization, *Geology*, 38(10), 875–878.
- 658 Ma, Z., E. Gray, E. Thomas, and B. Murphy (2014), Carbon sequestration during the Palaeocene-
659 Eocene Thermal Maximum by an efficient biological pump, *Nature Geoscience*, 7, 382-388..

- 660 Mahowald, N., M. Yoshioka, W. Collins, A. Conley, D. Fillmore and D. Coleman, (2006) Climate
661 response and radiative forcing from mineral aerosols during the glacial maximum, pre-industrial,
662 current and doubled-carbon dioxide climates, *Geophysical Research Letters*, 33(20).
- 663 Mancin, N., B. W. Hayward, I. Trattenero, M. Cobianchi, and C. Lupi (2013), Can the morphology of
664 deep-sea benthic foraminifera reveal what caused their extinction during the mid-Pleistocene
665 Climate Transition?, *Marine Micropaleontology*, 104, 53-70.
- 666 McCarren, H., E. Thomas, T. Hasegawa, U. Röhl, and J. C. Zachos (2008), Depth dependency of the
667 Paleocene-Eocene carbon isotope excursion: Paired benthic and terrestrial biomarker records
668 (Ocean Drilling Program Leg 208, Walvis Ridge), *Geochemistry, Geophysics, Geosystems*, 9(10),
669 1–10.
- 670 Melzner, F., J. Thomsen, W. Koeve, A. Oschlies, M. A. Gutowska, H. W. Bange, ... and A. Körtzinger,
671 (2013). Future ocean acidification will be amplified by hypoxia in coastal habitats. *Marine*
672 *Biology*, 160(8), 1875-1888.
- 673 Nguyen, T. M. P., and R. P. Speijer (2014), A new procedure to assess dissolution based on
674 experiments on Pliocene–Quaternary foraminifera (ODP Leg 160, Eratosthenes Seamount,
675 Eastern Mediterranean), *Mar. Micropaleontol.*, 106, 22–39.
- 676 Nguyen, T. M. P., M. P. Petrizzo, and R. Speijer (2009), Experimental dissolution of a fossil
677 foraminiferal assemblage (Paleocene-Eocene Thermal Maximum, Dababiya, Egypt): Implications
678 for paleoenvironmental reconstructions., *Marine Micropaleontology.*, 73(3), 241–258.
- 679 Nicolo, M. J., G. R. Dickens, C. J. Hollis, and J. C. Zachos (2007), Multiple early Eocene
680 hyperthermals: Their sedimentary expression on the New Zealand continental margin and in the
681 deep sea, *Geology*, 35(8), 699-702.
- 682 Nicolo, M. J., G. R. Dickens, and C. J. Hollis (2010), South Pacific intermediate water oxygen
683 depletion at the onset of the Paleocene-Eocene thermal maximum as depicted in New Zealand
684 margin sections, *Paleoceanography*, 25(4), PA4210.
- 685 Norris, R. D., S. K. Turner, P. M. Hull, and A. Ridgwell (2013), Marine ecosystem responses to
686 Cenozoic global change, *Science*, 341(6145), 492–8.
- 687 O'Connor, M. I., M. F. Piehler, D. M. Leech, A. Anton, and J. F. Bruno (2009), Warming and resource
688 availability shift food web structure and metabolism, *PLoS Biol.*, 7(8), e1000178.
- 689 Pälike, C., M. Delaney, and J. Zachos (2014), Deep-sea redox across the Paleocene-Eocene thermal
690 maximum, *Geochemistry, Geophysics, Geosystems*, 15(4) 1038–1053.
- 691 Panchuk, K., A. Ridgwell, and L. R. Kump (2008), Sedimentary response to Paleocene-Eocene
692 Thermal Maximum carbon release: A model-data comparison, *Geology*, 36(4), 315-318.

- 693 Penman, D. E., B. Hönisch, R. E. Zeebe, E. Thomas, and J. C. Zachos (2014), Rapid and sustained
694 surface ocean acidification during the Paleocene-Eocene Thermal Maximum, *Paleoceanography*,
695 29, 357-369.
- 696 Pörtner, H.-O., D. Karl, P. W. Boyd, W. Cheung, S. E. Lluch-Cota, Y. Nojiri, D. Schmidt, and P.
697 Zaviyalov (2014), Ocean Systems, in *IPCC WGII AR5*.
- 698 Post, J. E., Thomas, E., and Heaney, P. J., (in press) Jianshuiite in Oceanic Manganese Nodules. In
699 revision, *American Mineralogist*
- 700 Raffi, I., and B. De Bernardi (2008), Response of calcareous nannofossils to the Paleocene–Eocene
701 Thermal Maximum: Observations on composition, preservation and calcification in sediments
702 from ODP Site 1263 (Walvis Ridge — SW Atlantic), *Marine Micropaleontology*, 69(2), 119–138.
- 703 Raffi, I., J. Backman, E. Fornaciari, H. Pälike, D. Rio, L. Lourens, and F. Hilgen (2006), A review of
704 calcareous nannofossil astrobiochronology encompassing the past 25 million years, *Quaternary*
705 *Science Reviews*, 25(23), 3113-3137.
- 706 Ravizza, G., R. N. Norris, J. Blusztajn, and M. P. Aubry. (2001). An osmium isotope excursion
707 associated with the late Paleocene thermal maximum: Evidence of intensified chemical
708 weathering. *Paleoceanography*, 16(2), 155-163.
- 709 Ridgwell, A. J. (2001), Glacial-interglacial perturbations in the global carbon cycle, (Doctoral
710 dissertation, University of East Anglia).
- 711 Ridgwell, A. (2007), Application of sediment core modelling to interpreting the glacial-interglacial
712 record of Southern Ocean silica cycling, *Clim. Past*, (2001), 387–396.
- 713 Ridgwell, A., and D. N. Schmidt (2010), Past constraints on the vulnerability of marine calcifiers to
714 massive carbon dioxide release, *Nature Geoscience*, 3(3), 196–200.
- 715 Schneider, L. J., T. J. Bralower, L. R. Kump, and M. E. Patzkowsky (2013), Calcareous nannoplankton
716 ecology and community change across the Paleocene-Eocene Thermal Maximum, *Paleobiology*,
717 39(4), 628–647.
- 718 Schrag, D., D. DePaolo, and F. Richter (1995), Reconstructing past sea surface temperatures:
719 Correcting for diagenesis of bulk marine carbonate, *Geochimica et Cosmochimica Acta*, 59(11),
720 2265-2278.
- 721 Sexton, P. F., P. A. Wilson, and P. N. Pearson (2006), Microstructural and geochemical perspectives on
722 planktic foraminiferal preservation: “Glassy” versus “Frosty,” *Geochemistry Geophysics*,
723 *Geosystems*, 7(12).
- 724 Slotnick, B. S., G. R. Dickens, M. J. Nicolo, C. J. Hollis, J. S. Crampton, J. C. Zachos, and A. Sluijs
725 (2012), Large-Amplitude Variations in Carbon Cycling and Terrestrial Weathering during the
726 Latest Paleocene and Earliest Eocene: The Record at Mead Stream, New Zealand, *J. Geology*,
727 120(5), 487–505.

- 728 Sluijs, A. et al. (2006), S. Schouten, M. Pagani, M. Woltering, H. Brinkhuis, J. S. S. Damsté, ... and K.
729 Moran. (2006). Subtropical Arctic Ocean temperatures during the Palaeocene/Eocene thermal
730 maximum, *Nature*, 441(7093), 610–613.
- 731 Sluijs, A., Brinkhuis, H., Schouten, S., Bohaty, S. M., John, C. M., Zachos, J. C., ... & Dickens, G. R.
732 (2007a). Environmental precursors to rapid light carbon injection at the Palaeocene/Eocene
733 boundary. *Nature*, 450(7173), 1218-1221.
- 734 Sluijs, A., G. J. Bowen, H. Brinkhuis, L. J. Lourens, and E. Thomas (2007b), The Palaeocene – Eocene
735 Thermal Maximum super greenhouse : biotic and geochemical signatures , age models and
736 mechanisms of global change, edited by M. Williams, A. M. Haywood, F. J. Gregory, and D. N.
737 Schmidt, *Deep Time Perspectives on Climate Change: Marrying the Signal From Computer
738 Models and Biological Proxies*, 323-347.
- 739 Sluijs, A., S. Schouten, T. H. Donders, P. L. Schoon, U. Röhl, G.-J. Reichart, F. Sangiorgi, J.-H. Kim,
740 J. S. Sinninghe Damsté, and H. Brinkhuis (2009), Warm and wet conditions in the Arctic region
741 during Eocene Thermal Maximum 2, *Nature Geoscience*, 2(11), 777–780.
- 742 Sluijs, A., L. Van Roij, G. J. Harrington, S. Schouten, J. A. Sessa, L. J. Levay, G. J. Reichart, and C. P.
743 Slomp (2014), Warming, euxinia and sea level rise during the Paleocene-Eocene thermal
744 maximum on the Gulf Coastal plain: Implications for ocean oxygenation and nutrient cycling,
745 *Clim. Past*, 10(4), 1421–1439.
- 746 Solomon, S., G.-K. Plattner, R. Knutti, and P. Friedlingstein (2009), Irreversible climate change due to
747 carbon dioxide emissions., *Proceedings of the National Academy of Science U. S. A.*, 106(6),
748 1704–9.
- 749 Speijer, R., C. Scheibner, P. Stassen and A. M. M. Morsi, (2012). Response of marine ecosystems to
750 deep-time global warming: A synthesis of biotic patterns across the Paleocene-Eocene thermal
751 maximum (PETM). *Austrian Journal of Earth Sciences*, 105(1), 6-16.
- 752 Stap, L., A. Sluijs, E. Thomas, and L. Lourens (2009), Patterns and magnitude of deep sea carbonate
753 dissolution during Eocene Thermal Maximum 2 and H2, Walvis Ridge, southeastern Atlantic
754 Ocean, *Paleoceanography*, 24(1), 1–13.
- 755 Stap, L., L. Lourens, A. van Dijk, S. Schouten, and E. Thomas (2010a), Coherent pattern and timing of
756 the carbon isotope excursion and warming during Eocene Thermal Maximum 2 as recorded in
757 planktic and benthic foraminifera, *Geochemistry, Geophysics, Geosystems*, 11(11), 1–10.
- 758 Stap, L., L. J. Lourens, E. Thomas, a. Sluijs, S. Bohaty, and J. C. Zachos (2010b), High-resolution
759 deep-sea carbon and oxygen isotope records of Eocene Thermal Maximum 2 and H2, *Geology*,
760 38(7), 607–610.
- 761 Stassen, P., Thomas, E., and R. Speijer, (2015). Paleocene-Eocene Thermal Maximum environmental
762 change in the New Jersey Coastal Plan: benthic foraminiferal biotic events. *Marine
763 Micropaleontology*, 115: 1-23

764

765 Stein, R., B. Boucsein, and H. Meyer (2006), Anoxia and high primary production in the Paleogene
766 central Arctic Ocean: First detailed records from Lomonosov Ridge, *Geophysics Research Letters*,
767 33(18), 1–6.

768 Steineck, P., and E. Thomas (1996), The latest Paleocene crisis in the deep sea : Ostracode succession
769 at Maud Rise , Southern Ocean, *Geology*, (7), 583–586.

770 Thomas, E. (1998), Biogeography of the late Paleocene benthic foraminiferal extinction, in *Late*
771 *Paleocene-Early Eocene Climatic and Biotic Events in the Marine and Terrestrial Records*, edited
772 by A. M.P., L. S, and B. W. A, pp. 214–243, New York: Columbia University Press.

773 Thomas, E. (2003), Extinction and food at the seafloor : A high-resolution benthic foraminiferal record
774 across the Initial Eocene Thermal Maximum , Southern Ocean Site 690 ABSTRACT 80301(303).

775 Thomas, E. (2007), Cenozoic mass extinctions in the deep sea : What perturbs the largest habitat on
776 Earth?, *Geological Society of America Special Papers 424* (01), 1–23.

777 Thomas, E., and A. Gooday (1996), Cenozoic deep-sea benthic foraminifers: Tracers for changes in
778 oceanic productivity?, *Geology*, 24(4), 355-358.

779 Thomas, E., and N. J. Shackleton (1996), The Paleocene-Eocene benthic foraminiferal extinction and
780 stable isotope anomalies, *Geological Society, London, Special Publications*, 101(1), 401–441.

781 Thomas, E., and J. C. Zachos (2000), Was the late Paleocene thermal maximum a unique event?, *Gff*,
782 122(1), 169-170.

783 Tindall, J., R. Flecker, P. Valdes, D. N. Schmidt, P. Markwick, and J. Harris (2010), Modelling the
784 oxygen isotope distribution of ancient seawater using a coupled ocean–atmosphere GCM:
785 Implications for reconstructing early Eocene climate, *Earth and Planetary Science Letters*, 292(3-
786 4), 265–273.

787 Westerhold, T., U. Röhl, J. Laskar, I. Raffi, J. Bowles, L. J. Lourens, and J. C. Zachos (2007), On the
788 duration of magnetochrons C24r and C25n and the timing of early Eocene global warming events:
789 Implications from the Ocean Drilling Program Leg 208 Walvis Ridge depth transect,
790 *Paleoceanography*, 22(2), 1–19.

791 Westerhold, T., U. Röhl, and J. Laskar (2012), Time scale controversy: Accurate orbital calibration of
792 the early Paleogene, *Geochemistry, Geophysics, Geosystems*, 13(6), 1–19.

793 Winguth, A. M. E., E. Thomas, and C. Winguth (2012), Global decline in ocean ventilation,
794 oxygenation, and productivity during the Paleocene-Eocene Thermal Maximum: Implications for
795 the benthic extinction, *Geology*, 40(3), 263–266.

796 Zachos, J. C., D. Kroon, P. Blum, and Scientific Shipboard Party (2004a), Leg 208, Site 1262 Initial
797 Report, *Proc. Ocean Drill. Program, Initial Reports*, 208.

- 798 Zachos, J. C., D. Kroon, P. Blum, Scientific Shipboard Party, and S. S. Party (2004b), Leg 208,
799 Site1263 Initial Report, *Proc. Ocean Drill. Program, Initial Reports*, 208.
- 800 Zachos, J. C. J., U. Röhl, S. A. Schellenberg, A. Sluijs, D. A. Hodell, D. C. Kelly, and D. Kroon,
801 (2005), Rapid acidification of the ocean during the Paleocene-Eocene thermal maximum., *Science*,
802 308(5728), 1611–1615.
- 803 Zhou, X., E. Thomas, R. E. M. Rickaby, A. M. E. Winguth, and Z. Lu (2014), I/Ca evidence for upper
804 ocean deoxygenation during the PETM, *Paleoceanography*, 29, 964–975.
- 805 Ziveri, P., H. Stoll, I. Probert, C. Klaas, M. Geisen, G. Ganssen, and J. Young (2003), Stable isotope
806 “vital effects” in coccolith calcite, *Earth Planet. Sci. Lett.*, 210(1-2), 137–149.
- 807
- 808

809 TABLES

810

Experiment #ID	Interval: 0-40 ka			Interval: 40-65 ka			Interval: 65-100 ka		
	Interface dissolution	Bioturbation	Decreased saturation	Interface dissolution	Bioturbation	Decreased saturation	Interface dissolution	Bioturbation	Decreased saturation
STD	Y	Y	N	Y	Y	N	Y	Y	N
STD_sat	Y	Y	N	Y	Y	Y	Y	Y	N
STD_bio	Y	Y	N	Y	N	N	Y	Y	N
STD_satbio	Y	Y	N	Y	N	Y	Y	Y	N
ALT	N	Y	N	N	Y	N	N	Y	N
ALT_sat	N	Y	N	N	Y	Y	N	Y	N
ALT_bio	N	Y	N	N	N	N	N	Y	N
ALT_satbio	N	Y	N	N	N	Y	N	Y	N

811

812 **Table 1.**

813 List of (GENIE) Earth system modelling experiments. Shown are the combination of assumptions of:

814 (i) ‘interface’ dissolution model (otherwise ‘homogeneous’); (ii) bioturbation of upper sediment layers

815 (otherwise no vertical mixing); and (iii) reduced carbonate saturation, simulated by increasing the

816 pressure used in calculation carbonate saturation by the equivalent of 2000 m, that are applied to each

817 of 3 separate phases of the total 100 kyr of model simulation.

	1263					1262				
	<20 kyr	20-40 kyr	40-60 kyr	60-80 kyr	>80 kyr	<20 kyr	20-40 kyr	40-60 kyr	60-80 kyr	>80 kyr
Carbonate AR (g/cm ² /kyr)	2.811	1.362	0.475	2.058	3.831	11.160	0.232	0.394	1.426	2.45
Fine Fraction AR (g/cm ² /kyr)	2.905	1.548	0.624	2.165	3.922	1.309	0.392	0.514	1.503	2.380
Coarse Fraction AR (g/cm ² /kyr)	0.094	0.053	0.019	0.078	0.116	0.031	0.003	0.009	0.055	0.066
CF AR / FF AR	0.033	0.033	0.026	0.038	0.030	0.021	0.007	0.013	0.037	0.028
Planktic Foraminifera AR (#/cm ² /kyr)	4482	3271	1200	5367	13846	2123	78	927	5309	12313
Fragmentation ratio (%)	1.64	3.27	5.35	3.20	2.40	5.24	6.31	4.58	2.88	4.72

818

819 **Table 2.**

820 Absolute average values of sediment core characteristics, split into 20 kyr time periods, with 40-60 kyr

821 equating to the height of the ETM2 event.

822

823

824

825

Site 1262	%	Site 1263	%
<i>Nuttallides truempyi</i>	10.5	<i>Nuttallides truempyi</i>	10.9
<i>Quadrिमorphina profunda</i>	9.5	<i>Bulimina simplex</i>	7.7
<i>Nuttallides umbonifera</i>	6.2	<i>Abyssamina incisa</i>	7.4
<i>Bulimina kugleri</i>	5.8	<i>Oridorsalis umbonatus</i>	6.7
<i>Tappanina selmensis</i>	5.5	<i>Bulimina kugleri</i>	5.3
<i>Abyssamina poagi</i>	5	<i>Clinapertina complanata</i>	3.9
<i>Clinapertina complanata</i>	5	<i>Globocassidulina subglobosa</i>	3.5
<i>Oridorsalis umbonatus</i>	4.8	<i>Abyssamina sp.</i>	3.3
<i>Anomalinooides spissiformis</i>	4.2	<i>Pleurostomella acuminata</i>	3
<i>Fursenkoina fusiformis</i>	3.1	<i>Lenticulina muensteri</i>	2.9
<i>Epistominella exigua</i>	2.8	<i>Fursenkoina fusiformis</i>	2.6
<i>Pleurostomella acuminata</i>	2.8	<i>Clinapertina inflata</i>	2.4
<i>Nonionella robusta</i>	2.4	<i>Nonion havanense</i>	2.3
<i>Globocassidulina subglobosa</i>	2.4	<i>Siphonodosaria lepidula s.l.</i>	2.2
<i>Clinapertina inflata</i>	2.3	<i>Bulimina semicostata</i>	2.2
<i>Siphogenerinoides brevispinosa</i>	2	<i>Anomalinooides spissiformis</i>	2.2
<i>Abyssamina incisa</i>	1.9	<i>Aragonia aragonensis</i>	2.1
<i>Abyssamina quadrata</i>	1.8	<i>Cibicidoides mundulus group</i>	1.9
<i>Nonion havanense</i>	1.8	<i>Nuttallides umbonifera</i>	1.7
<i>Bolivinooides huneri</i>	1.6	<i>Nonionella robusta</i>	1.6
<i>Cibicidoides mundulus group</i>	1.5	<i>Vaginulina elegans</i>	1.4
<i>Bulimina simplex</i>	1.4	<i>Laevidentalina communis</i>	1.2
<i>Anomalinooides sp cf acutus</i>	1.4	<i>Quadrिमorphina profunda</i>	1.2
<i>Abyssamina sp.</i>	1.3	<i>Bulimina trinitatensis</i>	1.1
<i>Gyroidinooides mediceus</i>	1	<i>Alabamina dissonata</i>	1
		<i>Siphogenerinoides brevispinosa</i>	1
		<i>Stilostomella aculeata</i>	1

826

827 **Table 3.**

828 Most common taxa at Site 1262 and 1263, as percentage of the total number of specimens counted over
829 all samples at that site. The 27 species listed for Site 1263 and the 25 species listed for Site 1262 are
830 present at 1 % or more of that total population, all other taxa are less abundant.

831

832

833

834

835

836

837

838

PERCENT OF THE POPULATION										
	1263					1262				
	< 20 kyr	20-40 kyr	40-60 kyr	60-80 kyr	>80 kyr	< 20 kyr	20-40 kyr	40-60 kyr	60-80 kyr	>80 kyr
Rarefied number of species (100)	40	36.4	33.5	38.29	41.14	35.54	24.83	28.33	38.29	41.14
<i>A. poagi</i> %	0	0	0.15	0	0.04	3.63	11.87	8.47	0	0.04
<i>Q. profunda</i> %	0.77	1.06	1.19	0.86	2.76	4.78	9.41	10.01	0.86	2.76
<i>Clinapertina</i> %	5.49	6.68	10.23	6.95	4.78	14.06	20.38	10.83	6.95	4.78
<i>N. truempyi</i> %	8.91	11.54	11.91	11.94	11.49	9.28	7.57	14.79	11.94	11.49
<i>N. umbonifera</i> %	1.04	1.46	1.72	1.94	2.78	7	7.57	8	1.94	2.78
<i>N. truempyi</i> & <i>N. umbonifera</i> %	9.95	12.85	13.64	13.88	14.28	4.21	24.58	22.8	13.88	14.28
<i>A. aragonensis</i> %	2.28	1.22	0.89	2.97	1.82	25.96	1.57	0.19	2.97	1.82
<i>T. selmensis</i> %	0.7	0.52	0.35	0.47	1.55	7	1.46	2.93	0.47	1.55
<i>S. brevispinosa</i> %	1.4	0.93	0.22	0.97	1.15	4.21	0.25	0.36	0.97	1.15
<i>Buliminids</i> %	28.44	28.11	11.49	20.48	28.05	25.96	6.8	11.43	20.48	28.05
<i>Agglutinants</i> %	1.13	0.93	0.15	1.35	1.18	1.67	1.81	1.98	1.35	1.18
<i>Lenticulina</i> spp. %	5.21	5.15	3.88	5.85	4.95	0.06	0.05	0.05	5.85	4.95
<i>Lagenids</i> %	2.73	2.62	2.38	3.76	2.13	4.82	0.92	0.21	3.76	2.13
<i>Cibicidoides</i> spp %	3.41	3.22	2	3.31	3.57	2.05	4.76	3.84	3.31	3.57
<i>S. rugosa</i> %	0.34	0.06	0	0.47	0.25	9.22	0.66	0.05	0.47	0.25
<i>O. umbonatus</i> %	4.67	7.14	14.5	7.03	5.78	4.82	4.7	6.43	7.03	5.78
<i>G. subglobosa</i> %	4.32	3.1	1.91	3.91	2.88	1.15	5.06	3.82	3.91	2.88
Cylindrical Taxa %	9.99	9.2	14.78	12.82	11.51	9.22	2.6	4.16	12.82	11.51
<i>Buliminids</i> & Cylindrical taxa %	38.43	37.31	26.27	33.31	39.56	35.18	9.4	15.59	33.31	39.56
<i>E. exigua</i> %	0.71	0.69	0.44	0.11	0.22	1.15	3.03	2.52	0.11	0.22
BFAR	201.62	63.71	15.02	116.22	207.5	61.59	13.78	29.35	116.22	207.5

839

840 **Table 4.**

841 Average values of number of species, total benthic foraminifera accumulation rate (BFAR) and relative
842 abundances of individual benthic foraminifera species during the ETM2. The event is split into 20 kyr
843 time periods.

844

845

846

847

848

SPECIES SPECIFIC BENTHIC FORAMINIFERA ACCUMULATION RATES										
	1263					1262				
	< 20 kyr	20-40 kyr	40-60 kyr	60-80 kyr	> 80 kyr	< 20 kyr	20-40 kyr	40-60 kyr	60-80 kyr	> 80 kyr
<i>A. poagi</i> AR	0.000	0.000	0.042	0.000	0.641	0.525	0.016	0.053	0.612	0.596
<i>Q. profunda</i> AR	3.469	0.810	0.183	1.132	0.844	0.385	0.020	0.036	0.147	0.254
<i>Clinapertina</i> AR	0.374	0.108	0.015	0.180	0.476	0.119	0.023	0.032	0.275	0.330
<i>N. truempyi</i> AR	0.244	0.057	0.012	0.100	0.184	0.180	0.008	0.020	0.192	0.339
<i>N. umbonifera</i> AR	3.049	0.571	0.086	0.724	0.929	0.233	0.036	0.033	0.282	0.367
<i>N. truempyi</i> & <i>N. umbonifera</i> AR	0.218	0.051	0.011	0.085	0.147	0.413	0.004	0.012	0.108	0.171
<i>A. aragonensis</i> AR	1.058	1.144	0.141	0.711	1.265	0.058	0.073	0.098	0.599	0.722
<i>T. selmensis</i> AR	4.136	1.112	0.184	2.088	1.457	0.233	0.144	0.085	0.270	0.713
<i>S. brevispinosa</i> AR	1.902	0.671	0.465	1.233	3.149	0.413	0.204	0.773	3.014	5.120
<i>Buliminids</i> AR	0.069	0.023	0.012	0.059	0.074	0.058	0.024	0.022	0.072	0.114
<i>Agglutinants</i> AR	3.520	0.703	0.305	1.178	1.623	1.533	0.155	0.161	1.093	1.887
<i>Lenticulina</i> spp. AR	0.410	0.129	0.038	0.236	0.431	1.069	0.061	0.194	1.283	2.997
<i>Lagenids</i> AR	0.841	0.268	0.062	0.348	1.972	0.371	0.070	0.406	1.253	1.488
<i>Cibicoides</i> spp AR	0.817	0.316	0.086	0.362	0.713	0.880	0.039	0.073	1.047	2.542
<i>S. rugosa</i> AR	1.353	0.574	0.000	2.126	0.594	0.177	0.011	0.194	1.951	3.855
<i>O. umbonatus</i> AR	0.513	0.104	0.014	0.183	0.382	0.371	0.035	0.042	0.480	0.604
<i>G. subglobosa</i> AR	0.549	0.227	0.082	0.374	0.839	2.108	0.047	0.096	1.758	1.544
Cylindrical Taxa AR	0.204	0.073	0.012	0.094	0.185	0.177	0.063	0.064	0.185	0.378
<i>Buliminids</i> & Cylindrical taxa AR	0.051	0.017	0.006	0.035	0.052	0.043	0.017	0.016	0.051	0.087
<i>E. exigua</i> AR	3.422	1.071	0.316	1.365	1.939	2.108	0.064	0.153	0.571	0.364
Infaunal Taxa AR	0.045	0.015	0.005	0.029	0.047	0.043	0.017	0.016	0.051	0.087

849

850

851 **Table 5.**

852 Average values of species-specific benthic foraminifera accumulation rate (BFAR) during the ETM2.

853 The event is split into 20 kyr time periods.

854

855

856

857 **FIGURES**

858

859 **Figure 1.**

860 Illustration of the GENIE model grid for the late Paleocene / Early Eocene configuration, and showing
861 the distribution of wt % CaCO₃ in surface sediments at the end of the model spin-up phase (a) with the
862 location of Sites 1262 and 1263 marked by stars. Panel (b) illustrates the pattern of wt % CaCO₃
863 corresponding approximately to peak ETM2 conditions.

864

865 **Figure 2.**

866 The bulk carbon isotope record from the shallow and deep sites (a) using the age model of [Stap *et al.*,
867 2009], and (b) using our age model.

868

869 **Figure 3.**

870 Photographs of sections across the ETM2 event in two cores, from Site 1262 and Site 1263, from
871 Walvis Ridge ODP Leg 208, and the respective approximate sedimentation rates for the two sites, as
872 well as sediment lightness (color; Zachos *et al.*, [2004a, 200b]).

873

874 **Figure 4.**

875 Sedimentary response to ETM2; (a) Bulk $\delta^{13}\text{C}$, (b) Bulk $\delta^{18}\text{O}$, (c) CaCO₃ wt % [Stap *et al.*, 2009], (d)
876 Fine Fraction (< 63 μm) Mass Accumulation Rate (FF MAR), (e) Coarse Fraction (> 63 μm) Mass
877 Accumulation Rate, (f) ratio of Fine Fraction MAR/Coarse Fraction MAR, (g) Planktic Foraminiferal
878 Accumulation Rate (PF AR) and (h) Foraminifera Fragmentation Ratio (%).

879

880 **Figure 5.**

881 Biological response to the ETM2; (a) Benthic Foraminifera Accumulation Rate, BF AR, (b) rarefied
882 number of species (/100), (c – j) % abundance of individual benthic foraminifera species. Site 1263 %
883 abundances are not plotted during the peak event, because very few specimens were present
884 (Supplementary Information Data Set 1).

885

886 **Figure 6.**

887 Modelled increase in temperature at intermediate depths (~1500 m) minus the increase in temperature

888 in the deep ocean (~3500 m), given an increase in atmospheric CO₂ from (a) 1×PAL (pre-industrial
889 levels of atmospheric CO₂) to 2×PAL (b) 1×PAL to 6×PAL. (b) has been scaled to a doubling of CO₂
890 by multiplying a factor of 0.39. The stars show the approximate palaeo location of the Walvis Ridge
891 site (-11 degrees longitude by -33 degrees latitude). The simulations are from [Lunt *et al.*, 2010]. In
892 the absence of a circulation switch (Fig. 6a), at Walvis Ridge the warming is greater in the deep ocean
893 than in intermediate waters, whereas with a circulation switch (Fig. 6b) the warming is in intermediate
894 waters than in the deep ocean.

895 Panel c: conceptual evolution of temperature at the Walvis Ridge site through ETM2, from the model
896 simulations of [Lunt *et al.*, 2010]: temporal evolution of temperature at the surface (~5 m depth),
897 intermediate depths (~1500 m) and the deep ocean (~3500 m). It is assumed that the temperature is
898 that of the 2 × PAL simulation between 0 and ~40 kyr, then (following a circulation switch) the
899 temperature can be characterised by that of the 6 × PAL simulation for a period of ~40 kyr, then the
900 temperature reverts to the pre-switch state. The warming following the circulation switch is greater at
901 intermediate depths than in the deep ocean.

902

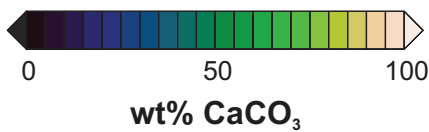
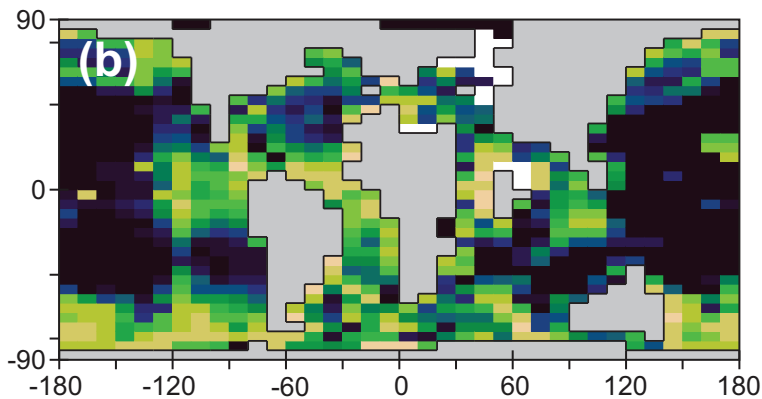
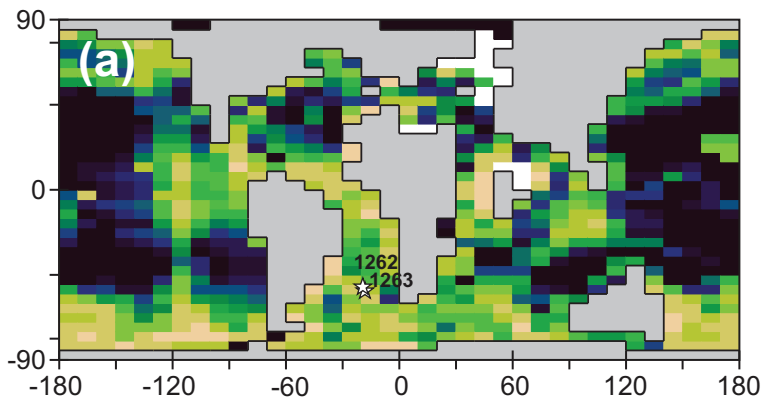
903 **Figure 7.**

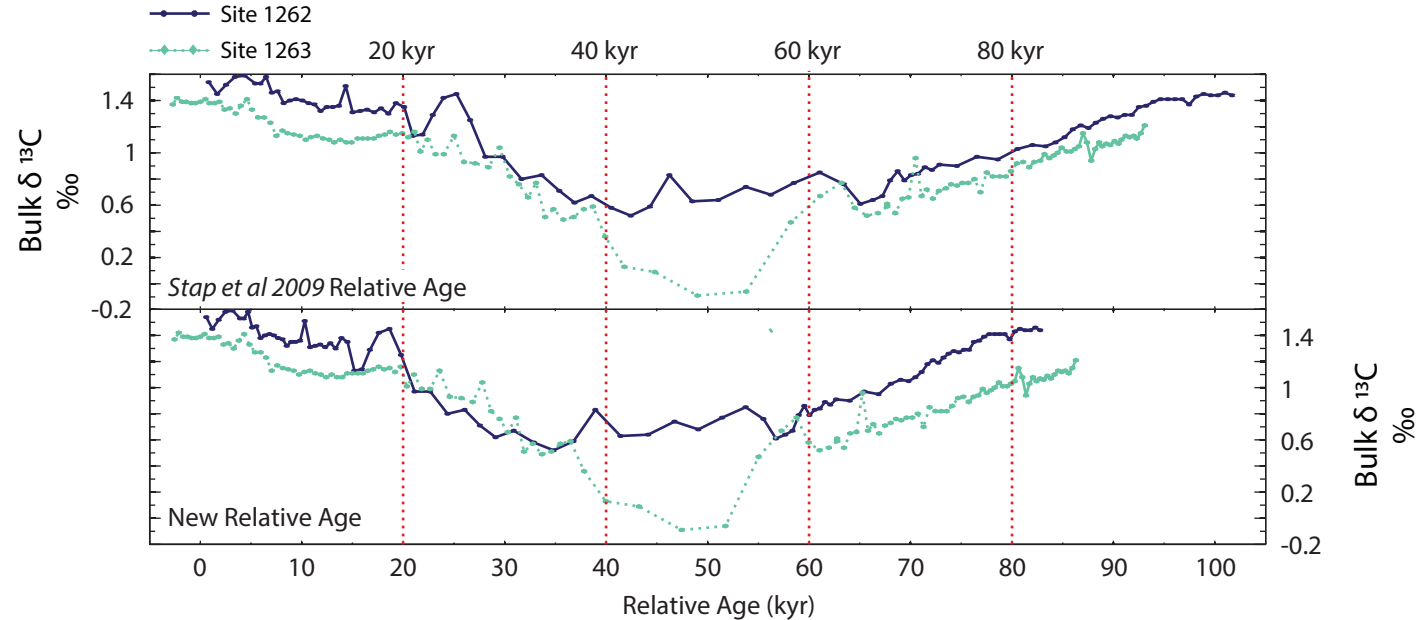
904 Model-predicted bulk sediment responses. Experiments show: bioturbational mixing, interface
905 dissolution occurring but no changing saturation state (STD), the same conditions with no interface
906 dissolution (ALT) and derivatives of this experiment with only a saturation state decrease during the
907 peak-event (ALT_sat), with only a shutdown of bioturbation during the peak-event (ALT_bio) and a
908 decreased of both bioturbation and saturation state during the peak-event (ALT_satbio).

909 Panel a shows the forcing applied to atmospheric CO₂ (LH axis) and to atmospheric δ¹³C_(CO₂) (RH
910 axis). The model time-scale runs from 20 kyr prior to the start of the perturbation experiments (i.e. the
911 last 20 kyr of the 200 kyr spin-up), and forward 100 kyr to the model experiment end. Time is plotted
912 relative to the start of the experiment – nominally equivalent to the onset of the ETM2 event (Figure 2)
913 with 0 kyr indicated by a vertical line.

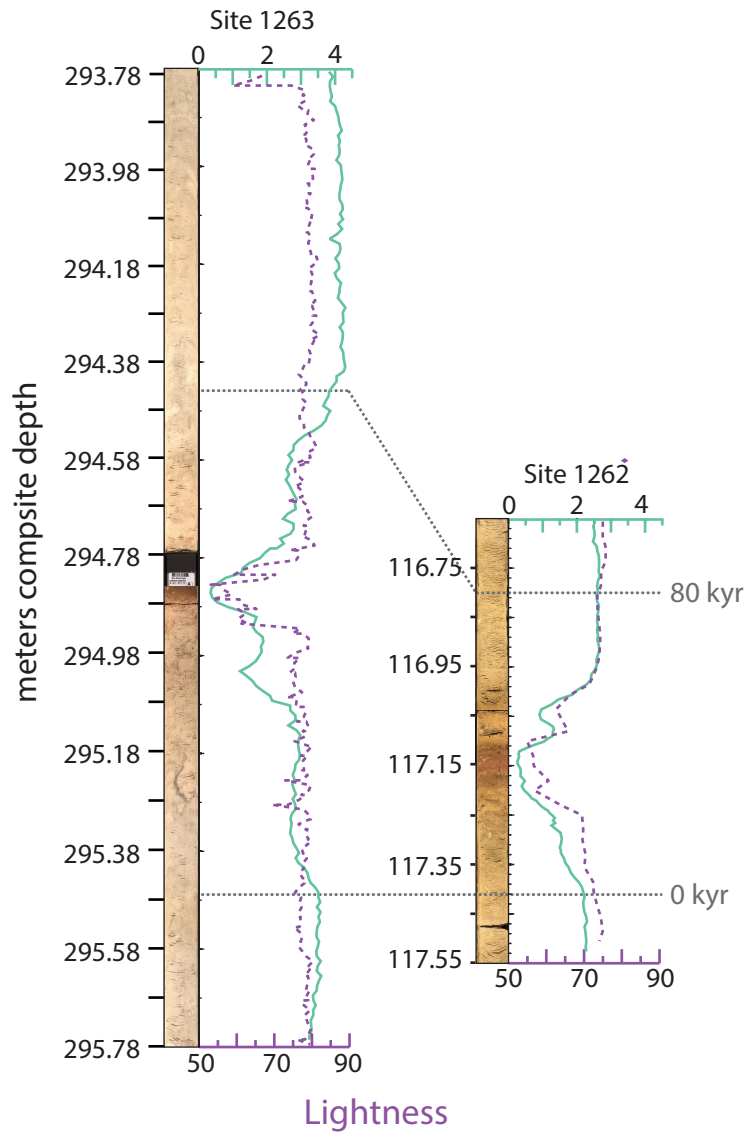
914 Panels b through g show the predicted evolution of bulk properties, with wt % CaCO₃ (yellow
915 symbols) on the LH axis and δ¹³C (red symbols) on the RH axis. The background color provides a
916 qualitative illustration of changing carbonate content (white == high wt % CaCO₃, red-brown == low
917 wt % CaCO₃). Of these: panels b and c show the simulated response at the model equivalent location to
918 Site 1262, and in panels d-g, for Site 1263. In panels e-g, the hatched region indicates the interval

919 throughout which there was no bioturbation (mixing) of the upper sediment layers in the model and/or
920 a greater pressure was assumed in calculating carbonate saturation (the 40-65 ka interval in Table 1).
921
922
923

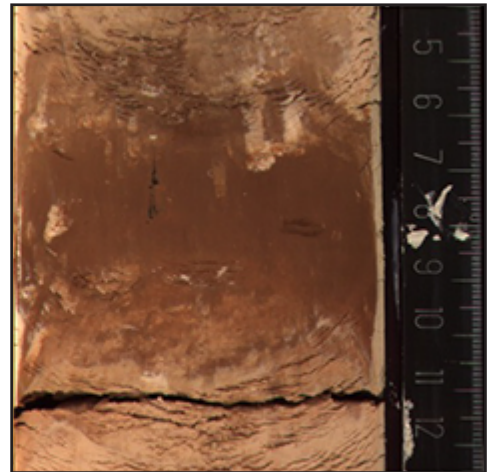




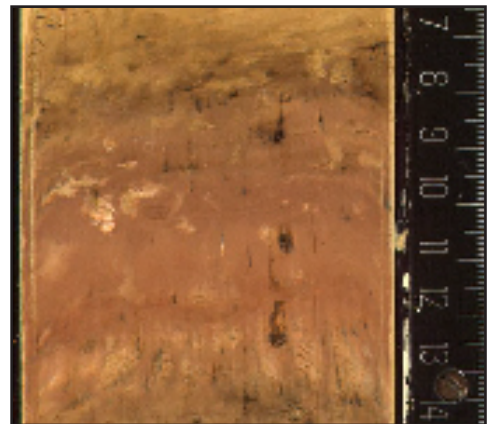
Sediment MAR (g/cm²/kyr)

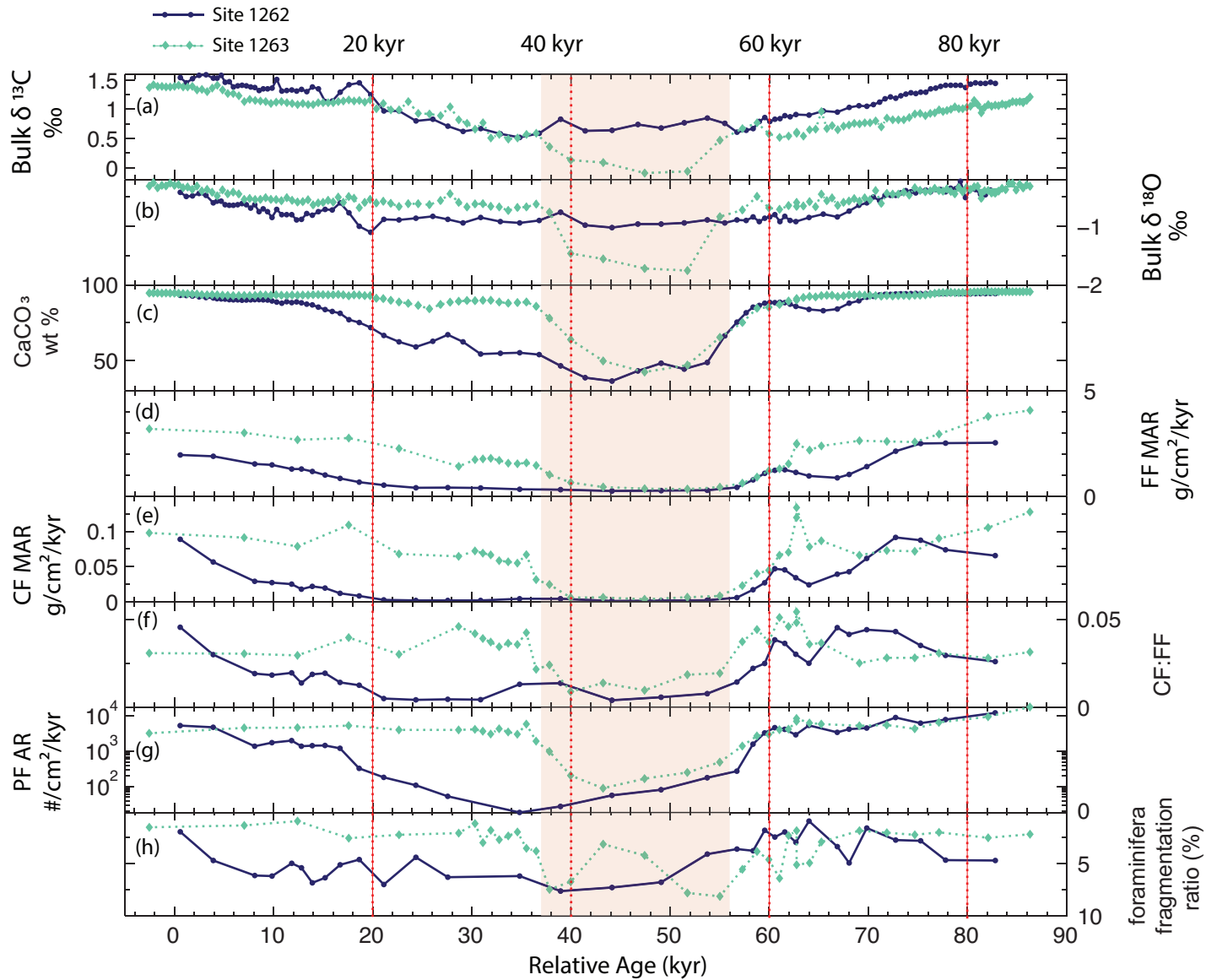


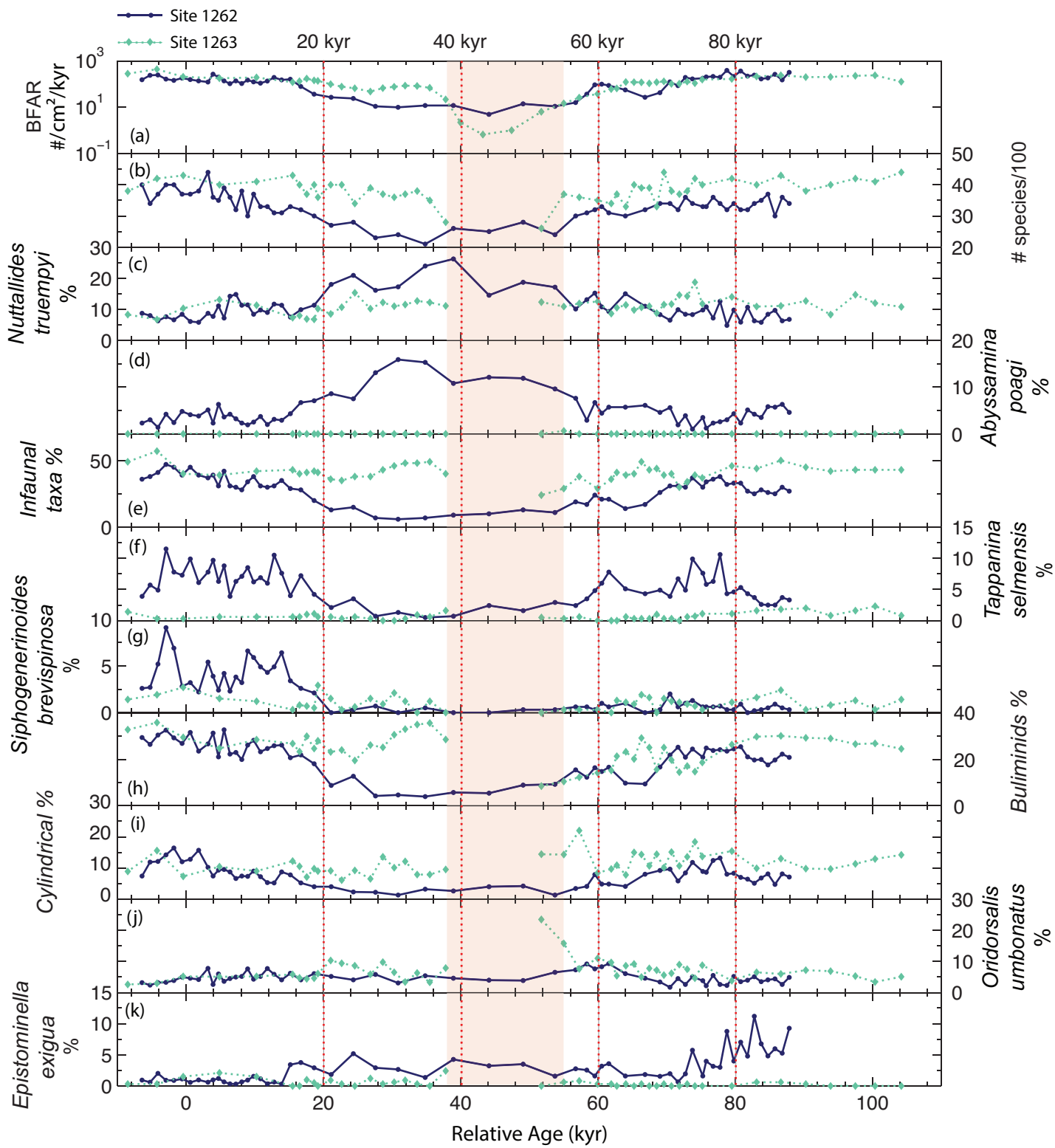
ETM2 horizon Site 1263

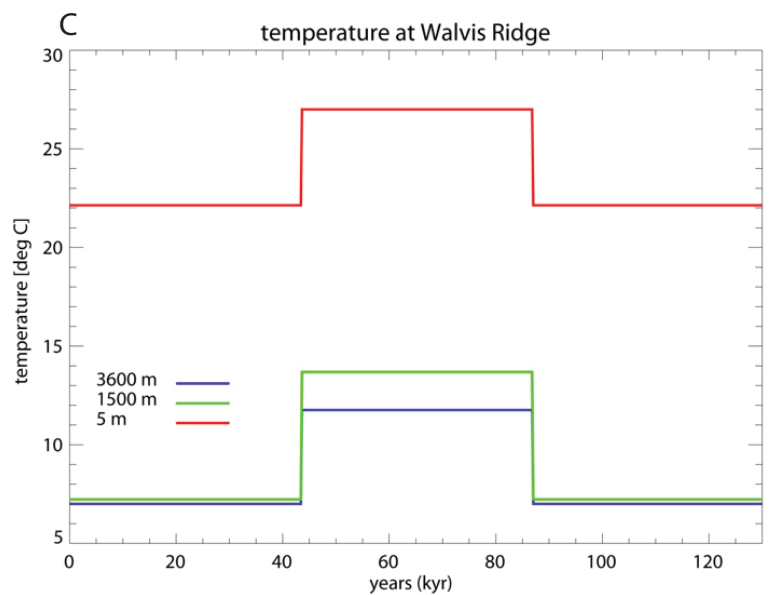
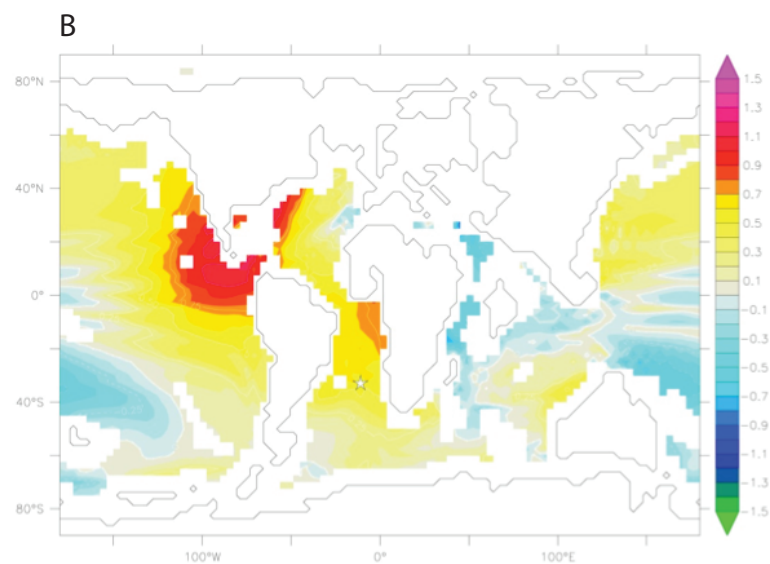
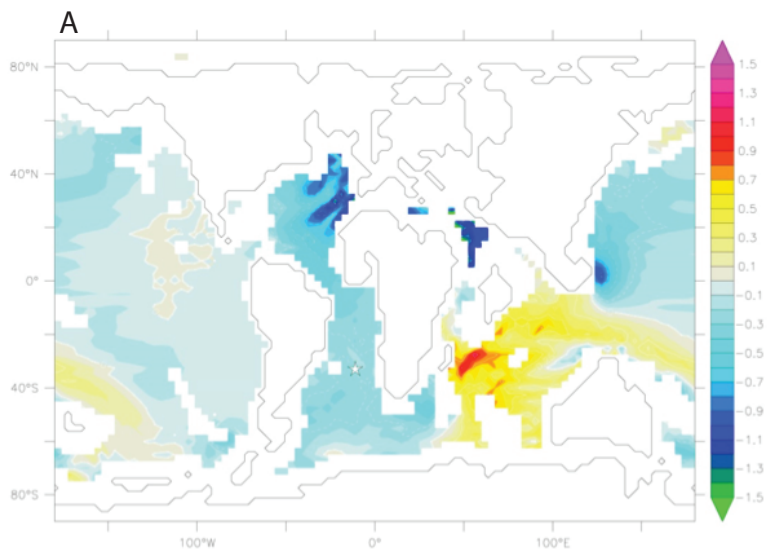


ETM2 horizon Site 1262

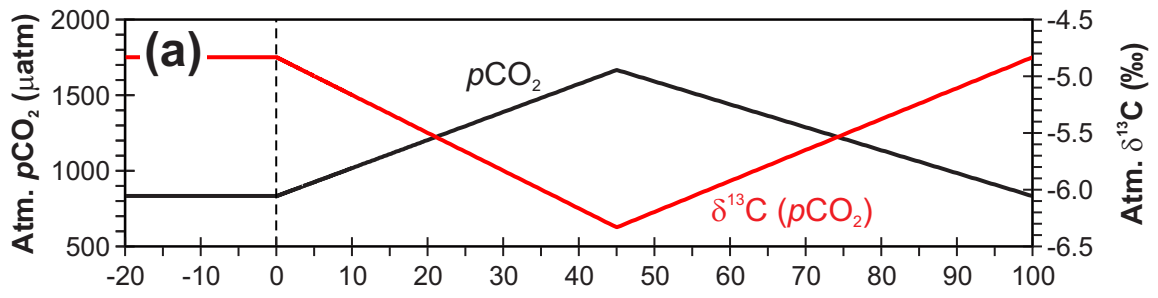




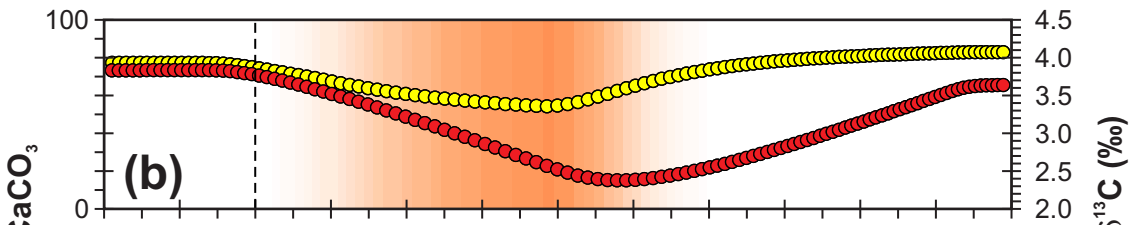




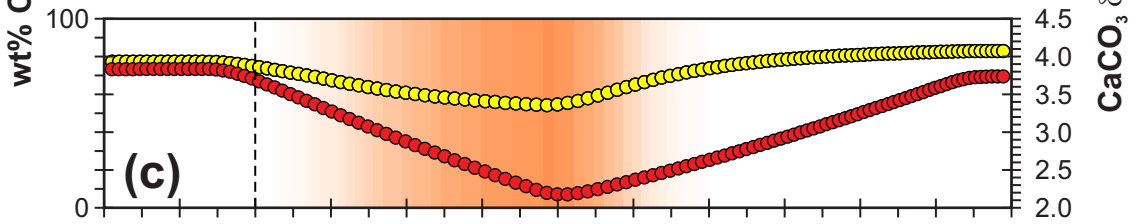
Atmospheric forcing



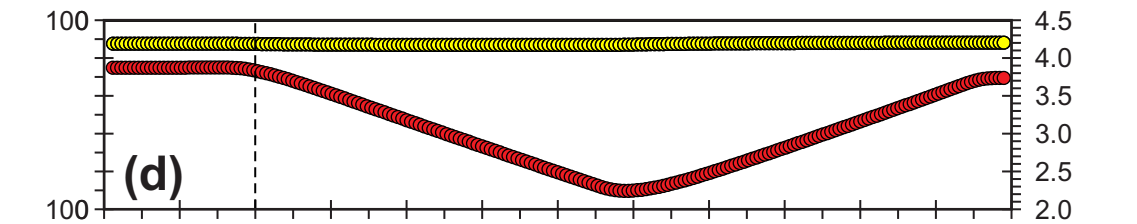
'STD'



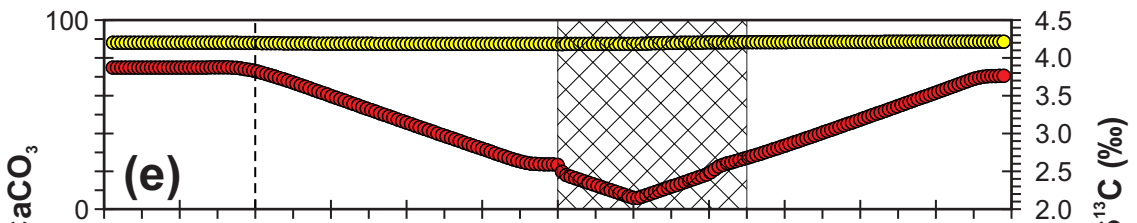
experiment 'ALT'



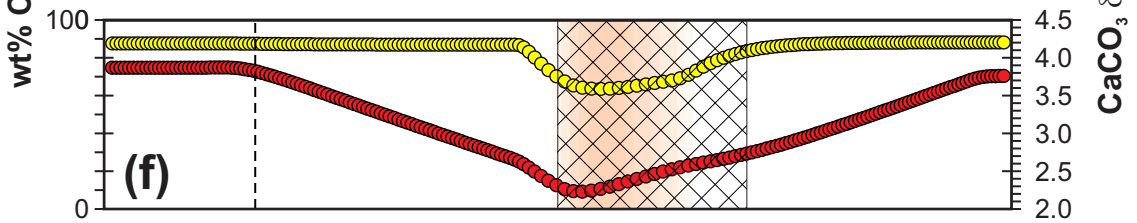
'ALT_bio'



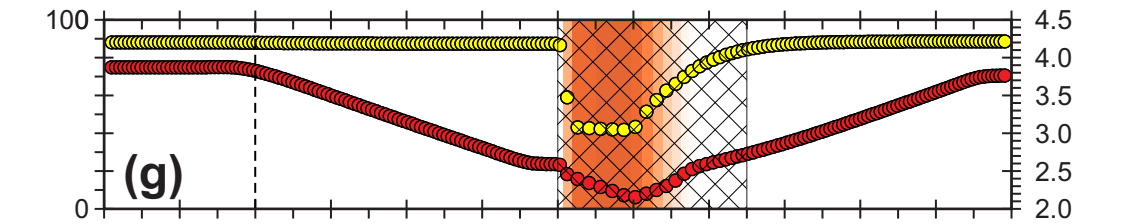
'ALT_sat'



'ALT_satbio'



'ALT_satbio'



Time since start of model experiment (ka)

- $\text{wt}\% \text{CaCO}_3$
- $\delta^{13}\text{C}(\text{CaCO}_3)$

'site' 1262

'site' 1263 simulated sedimentary response